remote sensing

MDPI

Article

Predicting Landslides Susceptible Zones in the Lesser Himalayas by Ensemble of Per Pixel and Object-Based Models

Ujjwal Sur [1], Prafull Singh [2], Sansar Raj Meena [3,*] and Trilok Nath Singh [4]

[1] Amity Institute of Geo-Informatics and Remote Sensing, Amity University-Sector 125, Noida 201313, India; ujjwal.sur@student.amity.edu
[2] Department of Geology, Central University of South Bihar, Gaya 824236, India; prafullsingh@cusb.ac.in
[3] Department of Geosciences, University of Padova, 35131 Padova, Italy
[4] Department of Earth Sciences, IIT Bombay, Mumbai 400076, India; tnsingh@iitb.ac.in
* Correspondence: sansarraj.meena@unipd.it

Abstract: Landslide susceptibility is a contemporary method for delineation of landslide hazard zones and holistically mitigating the future landslides risks for planning and decision-making. The significance of this study is that it would be the first instance when the 'geon' model will be attempted to delineate landslide susceptibility map (LSM) for the complex lesser Himalayan topography as a contemporary LSM technique. This study adopted the per-pixel-based ensemble approaches through modified frequency ratio (MFR) and fuzzy analytical hierarchy process (FAHP) and compared it with the 'geons' (object-based) aggregation method to produce an LSM for the lesser Himalayan Kalsi-Chakrata road corridor. For the landslide susceptibility models, 14 landslide conditioning factors were carefully chosen; namely, slope, slope aspect, elevation, lithology, rainfall, seismicity, normalized differential vegetation index, stream power index, land use/land cover, soil, topographical wetness index, and proximity to drainage, road, and fault. The inventory data for the past landslides were derived from preceding satellite images, intensive field surveys, and validation surveys. These inventory data were divided into training and test datasets following the commonly accepted 70:30 ratio. The GIS-based statistical techniques were adopted to establish the correlation between landslide training sites and conditioning factors. To determine the accuracy of the model output, the LSMs accuracy was validated through statistical methods of receiver operating characteristics (ROC) and relative landslide density index (R-index). The accuracy results indicate that the object-based geon methods produced higher accuracy (geon FAHP: 0.934; geon MFR: 0.910) over the per-pixel approaches (FAHP: 0.887; MFR: 0.841). The results noticeably showed that the geon method constructs significant regional units for future mitigation strategies and development. The present study may significantly benefit the decision-makers and regional planners in selecting the appropriate risk mitigation procedures at a local scale to counter the potential damages and losses from landslides in the area.

Keywords: landslide susceptibility mapping; modified frequency ratio (MFR); fuzzy analytical hierarchic process (FAHP); object-based geon method

Citation: Sur, U.; Singh, P.; Meena, S.R.; Singh, T.N. Predicting Landslides Susceptible Zones in the Lesser Himalayas by Ensemble of Per Pixel and Object-Based Models. *Remote Sens.* **2022**, *14*, 1953. https://doi.org/10.3390/rs14081953

Academic Editor: Fulong Chen

Received: 25 February 2022
Accepted: 12 April 2022
Published: 18 April 2022

1. Introduction

Landslide in the hilly terrain often accounts for substantial property and infrastructure damage, impacting people's livelihood. It is one of the most devastating complex geohazards. The fragile landscape of the Himalayan region is highly susceptible to landslides that pose a considerable risk to socio-economic setups and the means of support for the people residing there [1–3]. According to GSI (Geological Survey of India), about 140 thousand km^2 area in North-west Himalayas (Jammu and Kashmir, Himachal Pradesh, and Uttarakhand) is vulnerable to landslide hazards [4]. An estimate shows that nearly 13% of land in India has experienced landslides that caused more than USD 4.5 million economic loss [5,6].

Landslides in India's Uttarakhand state are considered one of the most threatening natural hazards, causing substantial damages and losses each year. Frequent landslides highly impact the middle and lesser Himalayas of Uttarakhand due to steep slopes, profound bedrock weathering, and intensive monsoon rainfall [7–11]. The anthropogenic reasons and geo-hydrological settings are the other vital elements that intensely stimulate landslide incidences [12,13]. Though numerous landslides occur every year in the mountainous northern part of Uttarakhand, the Varunawat landslide of 2003 is considered a significant event that caused a considerable loss of lives and properties [5,14]. Landslides in the Himalayas terrains are classified based on the size of the material displaced, categorized into debris flow, rockfall, mudflow, topples, soil creeping, and transitional slides by their predominant occurrences [15].

The Lesser Himalayan Kalsi-Chakrata road corridor observes considerable damages to structures and assets, road network, and occasional casualties from widespread rain-induced landslides in the rainy season (June to September). Such events incur economic losses and significantly impact villagers' livelihood in those mountainous terrains of the Lesser Himalayas. Many such landslide incidents have been published in national and local newspapers annually [16]. Amroha is the largest landslide in this road corridor located between Kalsi and Sahiya town. Over a decade, this landslide has recurred every year, resulting in passenger and goods transport disruption. The available literature reveals the absence of any in-depth scientific research on frequent landslides in this area [11]. Hence, filling the cavities and delineating the landslide-prone areas would be essential to conduct a detailed landslide susceptibility mapping (LSM) and analysis applying advanced geospatial techniques. Various techniques have been adopted in different studies worldwide, revealing other aspects of landslide prediction [17,18]. The LSM helps comprehend the distribution of likely landslide events spatially, which is a significant phase for landslide disaster mitigation and management in an area. The consistency and precision of LSM of a particular geographical unit depend on the spatio-temporal occurrence of landslides and the selection of the modeling approaches [19,20].

The advancement of satellite remote sensing (RS) and geographic information systems (GIS) technologies have meaningfully transformed the hazard mitigation planning perception for any future events [21]. The extensive application of RS and GIS techniques has emerged as a significant contributor for evaluating natural hazards [22–25]. RS and GIS have been used in many analyses for analyzing landslide susceptibility [11,26–28]. Landslides, floods, forest fires, and earthquakes are amongst the natural hazards that have been investigated widely using quite a few data-driven and heuristic models such as Frequency Ratio (FR), Analytic Hierarchical Process (AHP), and Evidence Belief Function (EBF) [29–33]. In this context, the physically-based landslide prediction models formulated on deterministic settings produced satisfactory results in some of the studies especially based on real-time data [34–37]. More recently, many 'machine learning' techniques have been used, such as Random Forest (RF), Support Vector Machines (SVM), Logistic Regression (LR), Dempster-Shafer, Decision Tree, and Artificial Neural Networks (ANN) [25,38–42]. Several studies have used FR or modified FR (MFR) model, a data-driven approach based on past landslide events, to generate landslide susceptibility maps [16,43–45]. On the other hand, satellite image analysis driven object-based image analysis (OBIA) has become a crucial method in GIScience [46]. In recent times, the machine-learning methods, namely naïve Bayes, naïve Bayes trees, were compared to MCDM (Multi-criteria Decision Making) techniques such as VIKOR, TOPSIS, and SAW. This result indicated higher prediction accuracy of ML techniques over the expert-based MCDM [20]. Recently, advanced ML methods with resampling algorithms are increasingly being used for landslide susceptibility assessment globally [35,47,48]. The ML and MCDM approach, though potent and often precise, must be considered to exhibit specific weaknesses and uncertainties. Often the shortcoming includes problems of overlearning, such as the appropriate selection of training sets that may impact the outcomes. In the context of the present study, some of the significant works on landslide susceptibility assessment in the road corridor has been carried out using

contemporary heuristic methods, statistical techniques and machine learning approach integrated with the Remote Sensing and GIS technique such as frequency ratio, the weight of evidence (WoE), evidential belief functions, AHP, statistical information value (SIV), logistic regression, random forest [49–55]. It was also noticed that many of the papers on road corridors in India adopted the FR and AHP methods for landslide susceptibility mapping [16,49,51,55].

In the present study, the LSI mapping in the Lesser Himalayan road corridor of Kalsi-Chakrata was conducted applying the per-pixel-based statistical/heuristic models (such as modified frequency ratio (MFR) and fuzzy-AHP (FAHP)), and object-based ensemble geon methods (such as geon MFR and geon FAHP) to delineate the landslide-prone areas. MFR and AHP/FAHP are popular contemporary techniques among the researchers for LSM in India particularly in the Himalayas. These LSM methods integrated with the use of low-cost high-resolution satellite data, and GIS techniques have yielded significant results in the past [44,56–59]. The MFR is a bi-variate model that helps to delineate the landslide susceptible areas correlating the past landslides and landslide causative factors; therefore, it omits the subjective biases such as knowledge-based weighted approaches [60–62]. Conversely, in recent times, advanced statistical methods, such as the FAHP, are presumed to be an instrumental methodology for MCDM [63]. The traditional AHP method is one of the most reliable criteria rating methods that use nearly crisp (non-fuzzy) decisions between factors through pairwise comparison in natural phenomena [16,64,65]. In complex natural systems, the decision-makers subjective judgments and uncertainties may significantly influence the process of policymaking. The fuzzy set theory integrated within the framework of AHP, employing fuzzy membership functions, permits more accurate results through greater flexibility for addressing the uncertainties and vagueness. We adopted the FAHP method recommended by Chang [66] using the geospatial technique to generate the LSM, and this method has been found significant for delineating the landslide susceptible zones in the Lesser Himalayas [11].

The object-based classification approach such as 'geons' based on image segmentation, on the contrary to the pixel-based approach, offers a more judicious answer for LSM [67,68]. Lang et al. [69] defined "Geons" as homogenous spatial units within a specific time and space that are driven by the policy and planning requirements for a particular region. The geon approach semi-automatically demarcates regions by incorporating the knowledge of experts. Any model can assess natural hazards depending on suitability, however, there are certain pros and cons associated with their accuracy and applicability over the former models. This is because the performance of a model varies considerably because of the data types, structures, and correctness, and hence it's a challenge for the researchers to select the appropriate model that can yield the best results for a specific area [70]. In this regard, it may be noted that the geon approach may be advantageous as it is formulated devoid of any administrative boundaries.

The study's primary goal is to compare landslide susceptibility mapping results obtained from the traditional yet straightforward per-pixel methodologies like MFR and FAHP and the ensemble object-based geons approach. This procedure would help understand which method is more suitable for LSM in the Lesser Himalayan Kalsi-Chakrata road corridor. This work's novelty is that it would be the first instance when the geon model will be attempted to delineate landslide susceptibility for the complex Himalayan topography as a contemporary LSM technique. Hence, it would be imperative to perceive if the object-based geon approach produces superior outcomes to the regular per-pixel approaches for the Himalayan terrain in India.

2. Study Area

The 42 km long road corridor connecting Kalsi with Chakrata lies in the Central Himalayas. This road corridor is located in the Dehradun district Uttarakhand state in India (Figure 1). While Chakrata (2118 m height above the mean sea level) is a well-known tourist place, Kalsi is a tiny cantonment town near the Yamuna. The study area experiences

three seasons namely winter (October to February), summer (March till June), and monsoon (June continues till September) with an average annual rainfall of about 1400 cm.

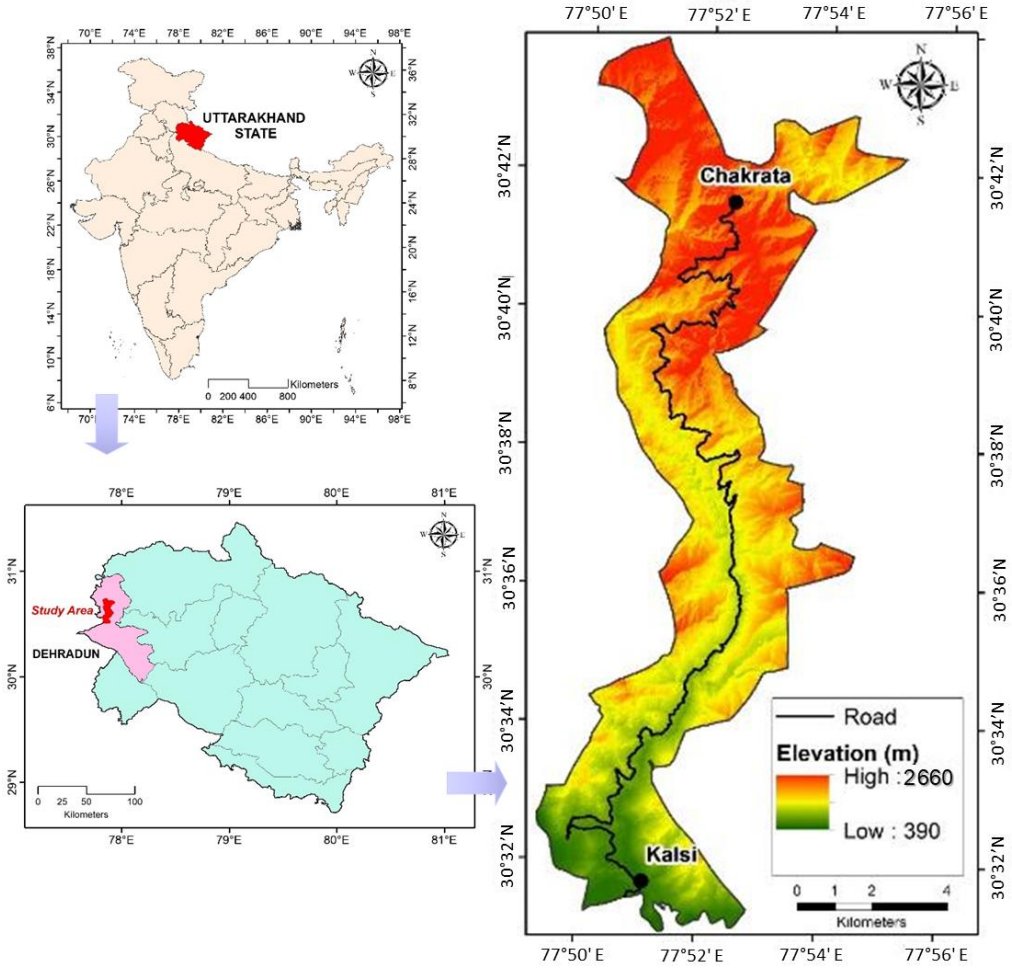

Figure 1. Location map of the study area.

The general lithology in the area mainly constitutes the Krol belt as the outer sedimentary belt, while the profuse sequences of un-metamorphosed sediments constitute the inner belt. The Himalayan main boundary fault (MBF) can easily be demarcated through the road corridor near Kalsi town making the area seismically active. The Kalsi-Chakrata road is passing through 33 villages and one municipal corporation (Chakrata). The study area has a total area of about 80 km^2 with a population of 19679 and a household of 3961 as per Census of India, 2011. Cultivation, community forestry, and tourism are some of the significant livelihoods of the villagers.

The detailed field investigations in the study area to specify debris flow, rock and debris slide, topple and rockfall, and rock slide as the main categories of rain-induced landslides (Figure 2a,b). Every year between June and August, due to heavy monsoon rainfall, the surface soils and rocks become saturated, resulting in many landslides due to slope failures. The landslides in the study area not only affect the villager's livelihood through direct damages to properties and infrastructure, and casualties, but eventually, influence the economy of the villagers by means of agricultural and business losses (rotten fruits and vegetables due to closure of transport routes). Such financial losses affect the communities' livelihood greatly in the study area. Overall, the combined impact attributable to the newer geologic formation, rugged terrain, heavy monsoonal rain, deep weathering, higher seismicity, and anthropogenic activities on unstable slopes in the area probably strongly correlate with the frequent landslides.

(**a**) (**b**)

Figure 2. Active landslides along the Kalsi-Chakrata road corridor, (**a**) Rock Fall between Chapanu and Sahiya, (**b**) Amroha landslide site in 2017, retaining wall damaged.

3. Materials and Methods

For performing the LSM, the initial step is to prepare a comprehensive inventory of the landslide database [71]. The standard methods to make such inventory include extracting information from the available landslide records or interpreting the higher resolution satellite data supported by intensive site exploration [7,72,73]. The next important step is to identify the crucial conditioning factors (geo-environmental factors) that might have triggered slope failure [74]. Terrain, slope angle, rainfall, lithology, road proximity are some of the crucial conditioning factors behind frequent landslides [35]. Such conditioning factors are often correlated with the landslide spatial occurrence using statistical or machine learning techniques in the predictive landslide models. More efforts have been made in the present study to prepare thematic conditioning layers in GIS from sources such as higher resolution satellite data, the latest vintage secondary data, or field survey observations captured through GPS instruments. A thorough literature review and record validation is a prerequisite before including data in the predictive hazard models. Table 1 presents the used in this study. The following sections present the sources of data along with resolution and vintage and materials used for generating landslide susceptibility maps.

Table 1. Details of thematic landslide conditioning factors.

Thematic Layers	Categories	Data and Sensor (Resolution/Scale/Vintage)	Data Source (Vintage)
Landslide inventory	Landslide records	Cartosat Satellite Image (2.5 m)	National Remote Sensing Centre (NRSC), [75]
		Linear Imaging Self-Scanning System IV (LISS-IV) (5.8 m), Resourcesat-2	
		Google Earth (2001–2017), Secondary data	Public Works Department (PWD), Geological Survey of India (GSI) portal [4]
DTM	Digital terrain model (DTM)	Cartosat 2.5 m, LISS IV (5.8 m)	NRSC (2017) [75]
Slope	Topographical	DTM (10 m)	NRSC (2017) [75]
Slope Aspect			
Altitude/Elevation			
TWI (Topographical wetness index)			
Lithology	Geology	Geological map (1:25,000)	GSI (2015) [4]
Proximity to faults			

Table 1. *Cont.*

Thematic Layers	Categories	Data and Sensor (Resolution/Scale/Vintage)	Data Source (Vintage)
Proximity to drainages	Hydrological	DTM (10 m), Toposheet (1:50,000)	NRSC (2017), SOI (2010) [75]
Stream power index (SPI)		DTM (10 m)	NRSC (2017) [75]
Rainfall	Meteorological	Rainfall records (past 60 years daily rainfall data)	Indian Meteorological Department (IMD) (1947–2017) [76]
Soil	Soil	Soil map (1:25,000)	National Bureau of Soil Survey (NBSS) (2010) [77]
Seismicity	Seismic	Seismic Zonation map (BIS), Average shear wave velocity at 30 m depth (Vs30)	Bureau of Indian Standards (BIS) (2002) [78] U.S. Geological Survey (2017) [79]
NDVI (Normalized Differential Vegetation Index)	Vegetation	LISS4 (5.8 m)	NRSC (2017) [75]
Land-use/ Land-cover (LULC)	Anthropogenic		
Proximity to road			

3.1. Mapping of Landslide Inventory

Mapping of Landslide inventory data presents the spatial distribution of past landslides and helps to identify various conditioning factors behind the incidence of a landslide. We used two primary sources to prepare the landslide inventory in this study: (i) past landslide data acquired from Uttarakhand PWD and (ii) marking of historical landslide scars from satellite images (LISS-IV and Google Earth satellite images). The collected records were mapped precisely after substantiation through extensive field surveys using the geotagged camera and GPS (Global Positioning System) device, laboratory investigations, and expert review. The field survey was conducted several times by the author between 2016 and 2020 covering the aspects of landslide inventory validation, collection of data on past landslide damages, investigation of possible triggering factors, socio-economic survey. The most common types of landslides in this area include debris slide, debris flow, rock slide, and rockfall (Figure 2). Since, there is no standard system for picking the training and test dataset for model building and validation, respectively, however, the typically used ratio of 70/30 has been adopted for training and validation samples [65,72]. Finally, the revised landslide inventory contained 107 landslide sites with descriptions of the past events and attributes such as size, length, etc. (Figure 3). The records were further randomly divided into 75 sites as a training dataset to develop the hazard model. About 71% of the training dataset was debris slide and flow, while 18% was rock slide, 11% was rock fall and topple. The 32 number remaining landslide inventories were considered for testing of model's precision, of which about 76% was debris slide and flow while the remaining 14% and 10% were rock slide and rock fall, respectively [11,58].

3.2. Landslide Conditioning Factors

Landslide conditioning factors essentially characterize the activating mechanism that possibly influences the landslide events in totality. Therefore, these are the factors that trigger the landslide events in combination in a complex natural environment. Based on specific site conditions, the number of these factors may differ, and the factors are chosen by a thorough literature review [10,64,80–83]. Their classification system and data acquisition process are directly associated with the nature of the conditioning factors and the related environment, their different natures, and regional environmental characteristics [84,85]. In this study, considering the complex hydro-geological and topographic setup of the Lesser

Himalayas, 14 such landslide conditioning factors were carefully chosen for the hazard models based on field investigation, literature, past experiences, and geospatial data available for the area [11,58,80]. These are slope angle, slope aspect, altitude, lithology, rainfall, NDVI, soil, seismicity, distance from road/drainage/fault, LULC, TWI, and SPI. Some of the above thematic layers were prepared from satellite images, while the remaining layers were generated from secondary sources at 10 m resolution using ArcGIS 10.1 software.

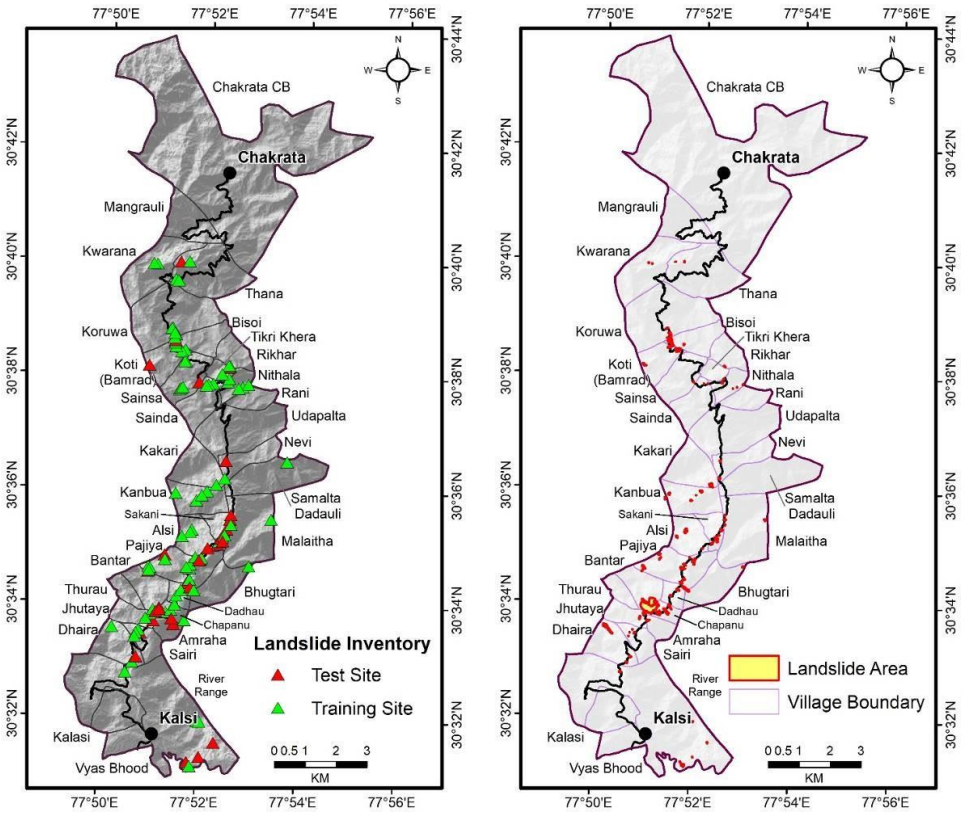

Figure 3. Landslide inventory along the Kalsi-Chakrata road corridor showing spatial distribution of (**a**) the test and training sites selected for model building, (**b**) landslide area in polygon.

The slope angle profoundly impacts the shear strength directly as the steeper slopes frequently generate more giant landslides as more materials are weathered and fragmented on such slopes [16,35,58,81,86]. The slope angle thematic layer in this study was prepared from Cartosat DTM. The slope angle layer was further divided into five distinct slope categories (<10°, 10–20°, 20–35°, 35–50°and, >50°) applying Jenk's Natural Breaks method; (Figure 4a). The slope aspect map, generated in ArcGIS by processing the Cartosat DTM, was classified into nine distinct sub-classes (Figure 4b). The difference in elevation or altitude may be interrelated with different environmental situations due to changes in rainfall, vegetation types, etc. The altitude thematic layer prepared from the DTM was categorized into five classes varying between 39 m near Kalsi and 2660 m near Chakrata (Figure 4c). Since no rainfall station is located in the said road corridor, the daily rainfall records for the eight surrounding district weather stations were obtained from IMD between 1947 and 2017 (past 70 years). The mean annual rainfall thematic layer was generated using the inverse distance weighted (IDW) interpolation method and categorized into five rainfall classes (Figure 4d). The geological map from GSI was used to prepare the lithological thematic data layer at 1:25,000 scale having eight distinct categories. Most of the past landslides happened in the areas under the Chandpur Formation and Mandhali-

Chakrata Formation from the lithological data. These are the formation along the road corridor that contains extensively weathered greywacke type of lithology (Figure 4e).

NDVI can significantly influence the occurrence of landslides as the steeper slopes lacking vegetation cover is more susceptible to erosion and slope failures [11,16,18]. The NDVI thematic layer in this study was prepared in ArcGIS software from LISS-IV satellite data. The NDVI thematic layer was then classified into five categories: −0.24–0.19, 0.19–0.31, 0.31–0.39, 0.39–0.48 and 0.48–0.77 (Figure 4f). The soil map of NBSS, India, was used to generate the thematic layer for soil. Four soil categories were generated as thematic layers based on the soil characteristics (soil texture, morphology, drainage condition). The analysis of the soil thematic layer indicates that the areas covered by coarse loamy soils on steep slopes (medium shallow, highly drained) experience more frequent landslides than the other classes (Figure 4g). Following the NRSC classification scheme, the LULC thematic layer was prepared after due validation and categorized into 14 LULC classes for the study area (Figure 4h). The road spatial data for the area was captured from LISS-IV data in ArcGIS software. It was the distance from the road that was calculated using ArcGIS software at every 100 m interval between 0 m and >500 m distance categories (Figure 4i) [11]. Similarly, to determine the effect of streams on the slopes, five drainage proximity categories were identified, each 100 m wide (Figure 4j). The tectonically active Himalayan Main Boundary Fault (MBF) has been observed to pass through the Kalsi-Chakrata road corridor. We have captured the major faults from the GSI geological map. The nearness to such a great fault zone may have a significant impact on the landslide occurrence. Five fault buffer zones (each 100 m wide) were generated (Figure 4k). The influence of seismicity on landslides is another critical factor considered in the Lesser Himalayas' landslide hazard models [11]. The seismicity thematic layer was generated by capturing details from BIS Seismic Zonation atlas in GIS, modified after USGS Vs30 data. Based on Jenk's natural break method, the seismicity layer was categorized into five classes showing peak ground acceleration values ranging from 3.5 m/s2 to 3.84 m/s2 (Figure 4l). TWI describes the effect of topography by detecting the water saturation areas having low slope gradient larger catchment. The output TWI was divided into 0–4, 4–8, 8–12, and 12–14 (Figure 4m). SPI data represents the erosive power of the streams. This thematic layer was calculated from the DTM and classified into two classes of 0–10 and 10–15 (Figure 4n) [11,16].

3.3. Landslide Susceptibility Mapping (LSM)

The index weights for selected landslide conditioning factors in this study were calculated through the Modified Frequency Ratio (MFR), and the fuzzy Analytic Hierarchy Process (FAHP) models applying geospatial techniques. Figure 5 illustrates the landslide susceptibility assessment methodology adopted along the Kalsi-Chakrata road corridor at 10 m × 10 m grid cells. The first step towards developing the landslide hazard models involves inventorying the past landslide events. Next, based on a thorough literature survey, the thematic layers were generated for the landslide conditioning factors. The thematic layers for 14 landslide conditioning factors were generated fusing GIS techniques for topographic, hydrologic, geologic, and anthropogenic elements. Using the selected contemporary statistical models, i.e., the MFR model and FAHP model, the LSI was calculated in GIS software following Equation (1), and finally, the validation of the landslide susceptibility maps of both the analysis was performed through ROC (Receiver Operating Characteristic) method using the training datasets.

$$LSI = \sum_{1}^{n} W \; and \; W = (wf_j \times wc_{ij}) \quad (1)$$

where, LSI = Landslide susceptibility index, W = Score of each class of a conditioning factor, $'wf'$ = Landslide factor criteria weight for factor $'j'$, and $'wc'$ = Criteria weight of class $'i'$ under conditioning factor $'j'$.

Using integrated RS and GIS technique, the LSI mapping for the models were carried out through the following steps:

(1) Landslide inventory preparation
(2) Identification of conditioning factors for landslide and generation of thematic layers
(3) Overlay of raster layers, conditioning factors, and past landslide events
(4) Calculation of FR values weightages/Computation of AHP weightages for the conditioning factors based on landslide cells and non-landslide occurrence cells.
(5) Calculation of MFR by normalizing the FR values/Computation of FAHP normalized weightages at the per-pixel level
(6) Generation of LSI maps by aggregating MFR/FAHP values
(7) Image segmentation using geons and aggregation of landslide susceptible zones
(8) Generation of object-based landslide susceptible zones applying geons approach
(9) Validation of the model results (refer to Section 5 for details)

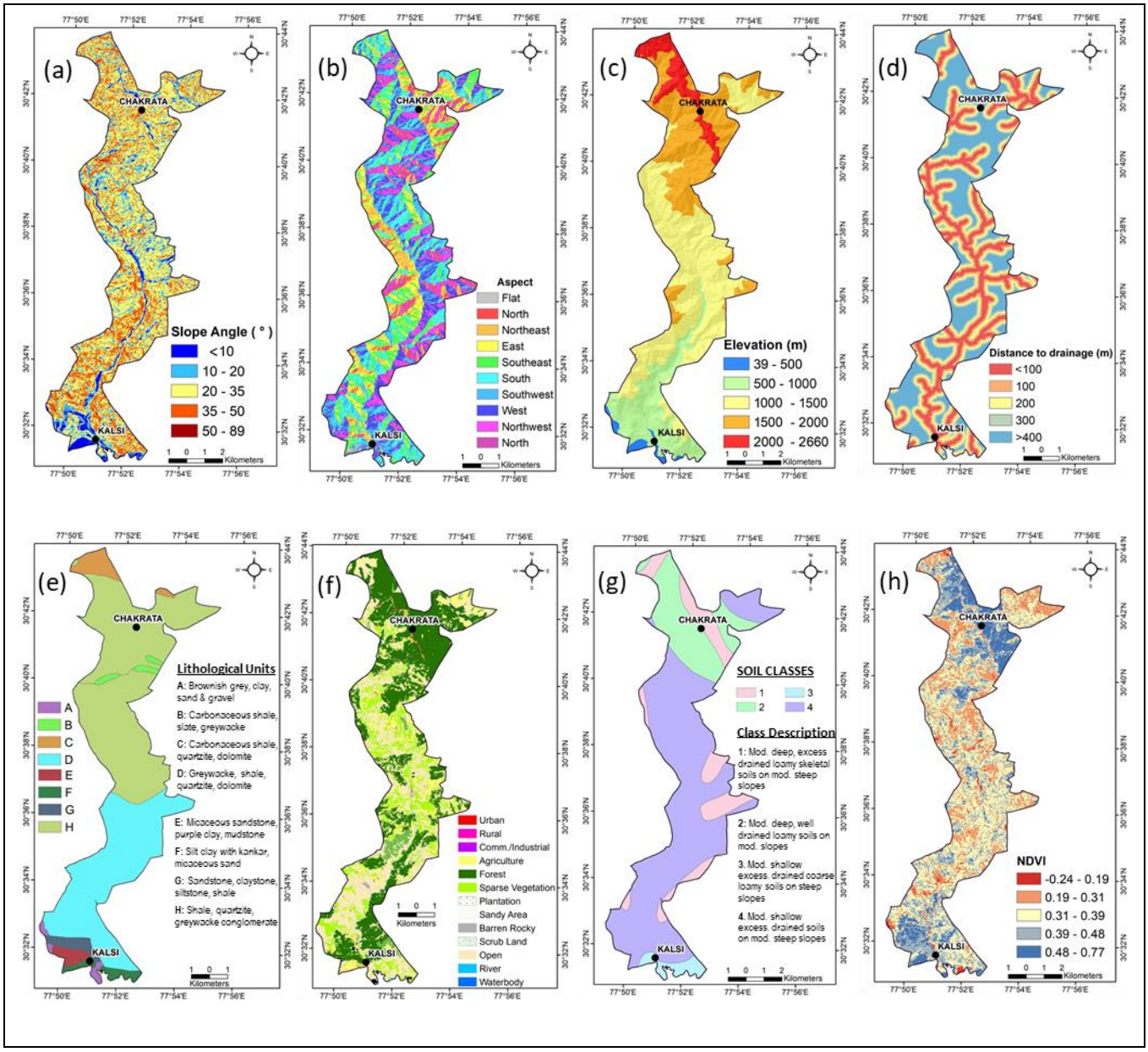

Figure 4. *Cont.*

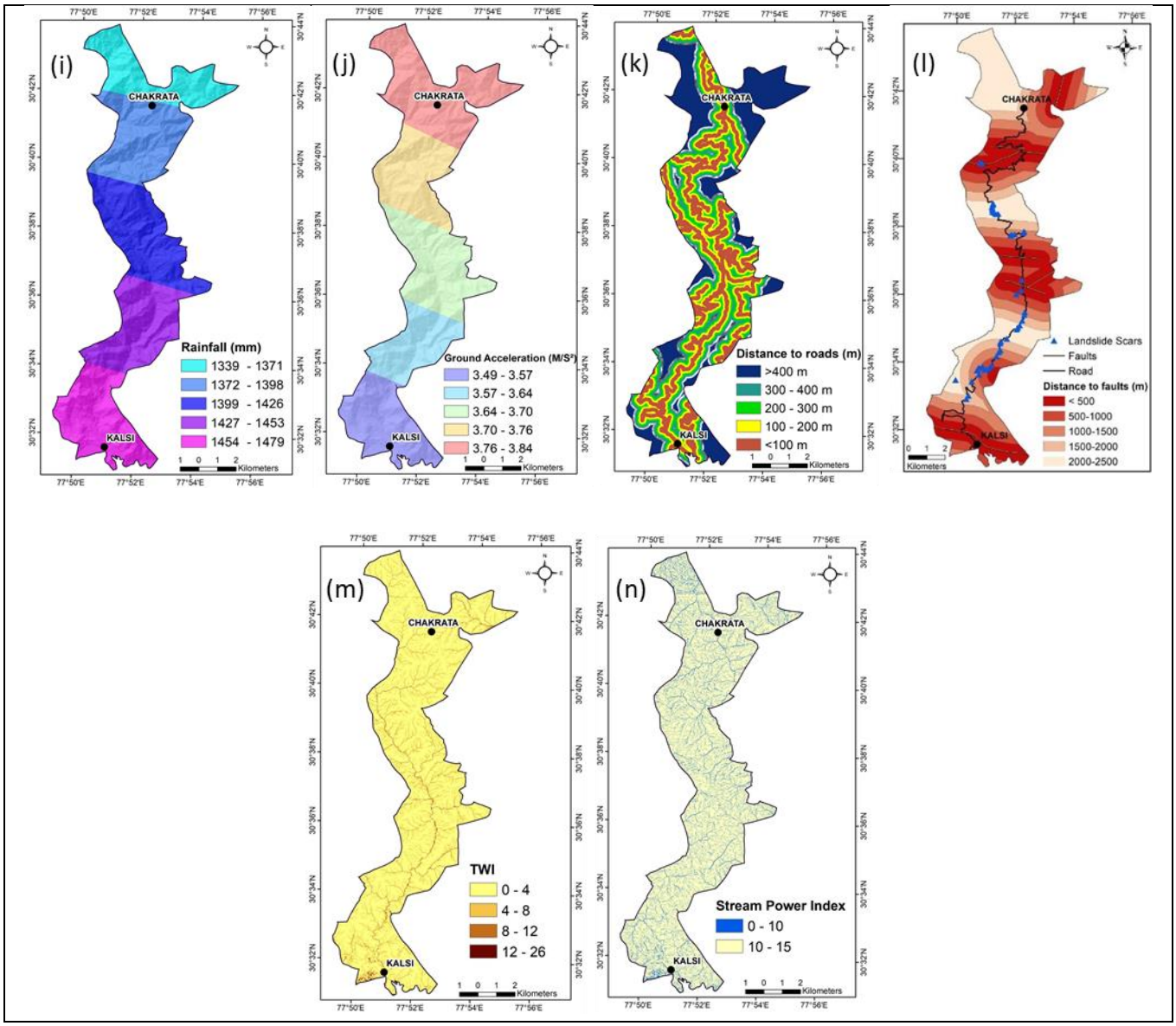

Figure 4. Landslide conditioning factors used in this study—(**a**) slope angle, (**b**) aspect, (**c**) elevation, (**d**) distance to drainage, (**e**) lithological units, (**f**) landuse/landcover (LULC), (**g**) soil, (**h**) NDVI, (**i**) rainfall, (**j**) seismicity, (**k**) distance to road, (**l**) distance to faults, (**m**) TWI and (**n**) SPI.

3.3.1. Weighting Approaches

Modified Frequency Ratio (MFR) Model

The Frequency Ratio is frequently and effectively applied leading probability model for Landslide Susceptibility Index (LSI) mapping [58,65,86]. The FR model is advantageous over many other LSI models as it can be implemented quickly, and its result shows a close resemblance with the actual situation on the ground [16]. The FR model is built on observed spatial associations between landslide conditioning factors and the occurrence of landslides in the past. Anticipating the hillside instability, the determination of the dependent variable is greatly influenced by the more independent variables [87].

In this study, the prejudice issue of the traditional FR approach has been rectified using a modified method that radically increases the continuity of the FR weighted values. The modified frequency ratio or MFR model is based on the factor value that can reveal the fluctuation of frequency ratio values due to categorization and can smoothen the spatial discontinuities [88].

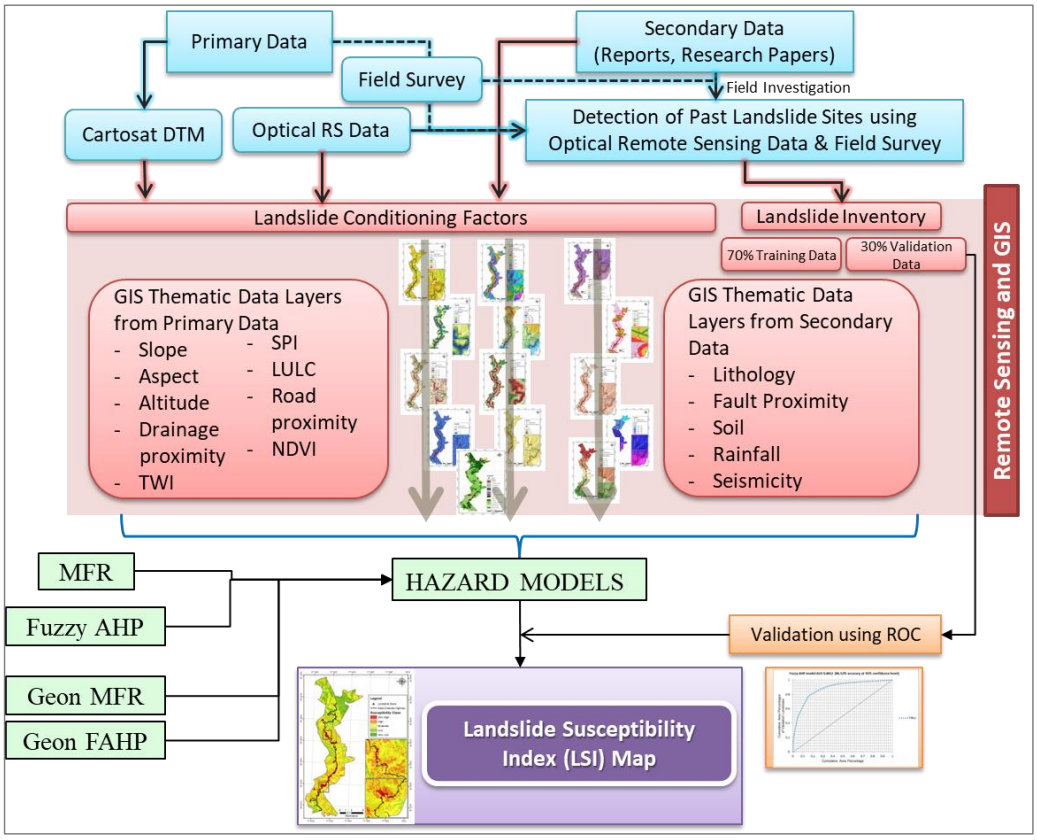

Figure 5. Methodology adopted for this study.

First, the calculation for FR values is carried out using the conventional method following Equation (2). For every landslide conditioning factor, FR value is calculated by the following formula after [72]:

$$FR_{m,n} = \frac{T_p(S_{m,n}) / \sum T_p(S_{m,n})}{T_p(N_{m,n}) / \sum T_p(N_{m,n})} \quad (2)$$

where, $FR_{m,n}$ = FR value of class n in factor m; $T_p(S_{m,n})$ is the pixel count of landslide occurrence within class n in factor m; $T_p(N_{m,n})$ is the pixel count of class n in factor m.

Now, applying the concept of MFR as shown in Equation (5), the ratios obtained in Equation (2) above are normalized to a range of 0–1. The RF (relative frequency) has been estimated using the following method for the i^{th} class [89,90]:

$$RF_i = \frac{FR_i}{\sum FR} = \frac{The\ FR\ of\ the\ i^{th}\ class}{\sum FR\ of\ the\ class} \quad (3)$$

Finally, the landslide susceptibility index (LSI) map was calculated using the MFR model applying the following equation by aggregating RF values of each factor [16,29] (Equation (4)). In an area, the higher landslide susceptibility is indicated by higher LSI and vice versa.

$$LSI = \sum RF \quad (4)$$

Fuzzy Analytic Hierarchy (FAHP) Process

The FAHP technique is an advanced MCDM statistical technique that implants the fuzzy theory within the framework of the traditional Analytic Hierarchy Process (AHP) developed by Saaty [65,91,92]. The concept of FAHP was first introduced by Laarhoven and Pedrycz [93]. The AHP method is primarily deployed in nearly crisp (non-fuzzy) decisions and does not consider the uncertainties associated with selecting pairwise comparisons.

In contrast, the FAHP model, in its place of AHP based definite ratings, allows picking intermediate pairwise comparison ratings for factors [94–96]. FAHP has been observed to depict better human skills, decisions, and rationale considering the complications in the natural systems [63,97]. The Chang's method of FAHP [66] was adopted to assess the landslide susceptibility through the following steps-

(1) Development of hierarchical structure: A judgment matrix was constructed for pairwise comparison of the linguistic variables on a scale of 1 to 9 where value 1 signifies 'equally important, while values of 3, 5, 7 and 9 denote 'slightly important, 'important, 'strongly important' and 'extremely important' hierarchies, respectively. The scale values, i.e., 2, 4, 6, 8, represented intermediate values between 1 and 3, 3 and 5, 5 and 7, 7 and 9, respectively. The decision-makers/scholars provided their judgments on a fuzzy triangular scale for selected criteria [11,98]. The consistency of the matrix judgments was thoroughly checked.
(2) Degree of membership and fuzzy matrix calculation: In this step, the scores of pairwise comparisons were converted into linguistic variables for determining the alternatives under the fuzzy environment.
(3) Computation of degree of possibility value: The fuzzy index weights, also known as degree of possibility value, were calculated at this step.
(4) Normalized fuzzy decision matrix: The normalized weights were calculated based on the maximum likelihood function.

3.3.2. Aggregation Approaches for Landslide Susceptibility Mapping

Geons (Object-Based Aggregation)

The resultant weights for various landslide factors were added at the pixel level in GIS software to determine the weighted LSI sum using the following equation,

$$\mathrm{LSI} = \sum_{t=1}^{n} W_t \, w_{st} \tag{5}$$

where, n shows the number of parameters; for conditioning factor 't', W_t and w_{st} depict the normalized FAHP value and sub-class 'st' weighted value.

The word "geon" comes from the Greek gē (Γῆ) = lan, earth, and the suffix -on for anything existing. Geons, according to Lang et al., are a form of territory that is delineated semi-automatically using expert knowledge. These zones are scaled and uniform in response to a phenomenon that is a source of policy concern in space [69]. Geons are generally separate spatial units with varied space-time occurrences that are homogeneous [65]. It defines geon as a spatial entity that is scale-dependent. Through vector encoding, such an object has stability qualities such as decreased inherent variance and gradients towards the outside [69,99].

To accomplish domain-specific (i.e., based on experts) and semi-automatic regionalization, the geon approach operates in a bipartite course. In general, geons use a complex mapping method to create composite objects, which includes data analytic and taxonomic procedures [69,100]. Image segmentation based on spatial continuousness and certain homogeneity criteria is used in the geon technique to conduct multi-component regionalization [65].

Multi-resolution segmentation (MRS) is a widely used approach in object-based analysis (OBIA) that constructs homogeneous picture segments inside a tiered hierarchy of scaled representations [101,102]. MRS starts at the pixel level and aggregates into objects of various forms, sizes, and attributes until it reaches a homogeneity threshold determined by the user. The accumulation of spectral information in this manner helps to reduce the loss of details [103]. Making geons has the goal of preparing a geographical phenomena that are connected to policy and adaptively validated by experts. As a result, they make it easier to see, forecast, and comprehend the geographical distribution of landslide susceptibility in a given area, as well as help in improved mitigation planning [104]. eCognition software was used to segment and parameterize the images, and the landslide conditioning

factors were transformed to 8-bit data (GeoTIFF format) with cell values standardized between 0 and 255. The normalization was carried out based on Equation (6):

$$Vi = \frac{V - Vmin}{Vmax - Vmin} * 255 \quad (6)$$

where, V_i is the normalized 8-bit value, V is the landslide conditioning factor value, Vmin and Vmax present the minimum value and the maximum value of the entire data range for the V layer.

In this regard, it should be highlighted that the scaling parameter (SP) choices are the primary source of concern in MRS. The Assessment of Scale Parameter tool (ESP) uses a single layer to find the optimum scales produced on a local variance graph [104]. This ESP2 is a fully automated approach for selecting multiple-layer scale settings [105]. In this study, we used the eCognition Developer software to acquire the optimal scale values applying the MRS concept. The finest scale was used for generating the geons.

3.4. Model Validation and Evaluation

In any LSM analysis, model validation and analysis of the results are crucial [21]. Therefore, the resulting LSM from the selected models was compared against the landslide test data (30% validation datasets) to determine correctness. This method intends to assess the effectiveness of each LSM model, particularly whether those can correctly predict the landslide susceptible areas [65,106].

3.4.1. Receiver Operating Characteristics (ROC)

We validated the four LSM output derived from the MFR, FAHP, geon MFR and geon FAHP models through the ROC curve by means of validation or test data by correlating the false alarm probability against the detected probability [27,107]. The AUC (area under the curve) analysis specifies the degree that indicates the model's LSM output precision. More the AUC values entitle a higher accuracy of the model adopted and vice versa [11,65].

3.4.2. R-Index (Relative Landslide Density)

The model's prediction capability in this study was also verified through the R-index method. This validation method indicates the spatial correlation between landslide test records and the LSI values [11,27]. The R-index was calculated through the following equation-

$$R = (a_i/A_i)/\sum(a_i/A_i) \times 100 \quad (7)$$

where,

A_i = the % of landslide susceptibility area in each LSM class;

a_i = the % of landslide counts in each LSM class.

4. Results and Analysis

4.1. Per-Pixel Based MFR and FAHP Analysis

As illustrated in the methodology, the final weightages for the MFR and FAHP were calculated for each conditioning factor after normalization (Table 2). By integrating the final factor weightages for MFR and FAHP at the per-pixel level in ArcGIS software, the LSM was generated. (Figure 5). The main focus of adopting the MFR and FAHP approaches is to emphasize the spatial LSM for the study area for future developmental planning and mitigation.

In the absence of a standard taxonomy for classifying the LSI values, the output of both MFR and FAHP models were mapped through Jenk's Natural Breaks method into Very Low, Low, Moderate, High, and Very High landslide susceptibility classes. Higher LSI values contain the areas falling into higher landslide susceptibility zones and vice versa. To better predict the probability of future landslides spatially, this study indicates the landslide

conditioning factors and their connection with each other in triggering the landslides in the study area.

The landslide susceptibility assessment obtained from the MFR approach shows that very high and high landslide susceptible zones cover about 9.9 km^2 (12%) and 20.9 km^2 (25%) of the road corridor, respectively (Table 2). Further, it has also been noted that LSI zones having moderate landslide susceptibility probability cover about 22.4 km^2 (27%) of the total area. Therefore, future landslides may be more likely in similar areas with moderate susceptibility without intermittent observations, sustainable approach, and future investigation.

The output of the FAHP model shows that the areas under high and very high susceptibility cover about 45.23 km^2 (55% of the study area). In contrast, 17.7 km^2 (21%) of the total area falls under the very high LSI category. The moderate landslide susceptible zone covers about 17.6% (14.5 km^2) of the total village areas. In particular, the moderately susceptible zones without appropriate mitigation measures may have a higher possibility of future landslides (Figure 6).

Further, the spatial assessment at the village level was performed to recognize the nature of the landslide hazard (. Such an approach helps to mitigate landslide hazard risks and minimize the damages and losses locally. The analysis of the MFR model showed that Dadhau village and Jhutaya village in the study area are the utmost vulnerable to potential landslide hazards, with about 65% and 53% of their respective areas being contained by very high LSI zone. Apart from these, the villages having greater exposure to very high landslide susceptibility are Chapanu (64%), Pajiya (52%), Malaitha (39%), and Alsi (38%). Considering combined areas under both very high and high landslide susceptibility zones, Dadhau village has more than 90% of its geographical area under higher landslide hazards, followed by Chapanu (88%), Pajiya (87%), Sakani (85%), and Bantar (81%). For the FAHP model, it was observed that Nevi village is most susceptible to landslides. This village is near Sahiya town, with 62% of its areas under very high landslide hazard. Chapanu, Kanbua, Pajiya, and Kakari are among the other villages with a higher percentage of village areas under the very high landslide hazard zones. Considering both the MFR and FAHP models, the analysis showed that Dadhau, Nevi, Jhutaya, Chapanu, Pajiya, and Dhaira villages are more susceptible to very high landslide hazards.

4.2. Per-Pixel and Object-Based Geons Result Analysis

As described in the methodology section of this paper, the output LSI from the MFR and FAHP approaches were processed using the segmentation algorithm of "geons" to generate the homogenous LSM units in eCognition software. Figures 7 and 8 presents the spatial analysis of the MFR geons and FAHP geons output for the Kalsi-Chakrata road corridor. Similar to the LSM classification from the per-pixel approach, the thematic LSM layer from geon was also categorized into five distinct classes based on Jenk's natural break technique.

The landslide susceptibility assessment obtained from the geon MFR approach shows that about 5.69 km^2 (6.9%) and 25.56 km^2 (30.9%) fall in very high and high out of the whole study area LSI zones, respectively. Further, it has been noted that the moderately susceptible zone accounts for about 21.55 km^2 (26%) of the total area. Therefore, these areas might experience landslide events in the future without appropriate developmental planning, sustainable approach, and in-depth investigation (Figure 7).

The output of the geon FAHP approach shows that out of the whole study area, about 13.74 km^2 (16.6%) and 20.70 km^2 (25%) areas have been categorized into higher landslide susceptibility (under very high and highly susceptible zones), respectively. Further, about 22.36 km^2 (27%) area falls within moderately susceptible zones as per the geon FAHP model (Figure 7). It has also been observed that both geon MFR and geon FAHP approaches depict similarity in the delineation of very low landslide susceptible areas (9.2% of the whole areas for MFR and 8.6% of the entire study area for FAHP).

Table 2. Normalized weightages for MFR and FAHP models.

Factor	Unit	Class	Class	Landslide	Frequency Ratio (FR)	MFR	FAHP		Consistency Ratio
			%	%			Weights	Factor Weights	
Slope	Degree	0–10	34%	1%	0.03	0	0	0.11	0.0067
		10–20	29%	7%	0.23	0.02	0.01		
		20–35	4%	2%	0.56	0.06	0.03		
		35–50	27%	46%	1.74	0.18	0.03		
		50–89	6%	44%	7.26	0.74	0.04		
Aspect	Class	Flat	5%	0%	0	0	0.003	0.093	0.003
		North	13%	0%	0	0	0.01		
		NE and NW	33%	1%	0.02	0	0.014		
		S and SW	5%	54%	10.18	0.82	0.025		
		E and SE	23%	9%	0.38	0.03	0.018		
		SE	20%	37%	1.8	0.15	0.023		
		39–500	8%	0%	0.014	0	0.006		
Altitude	Meter	500–1000	21%	44%	2.056	0.64	0.008	0.055	0.002
		1000–1500	51%	56%	1.103	0.34	0.013		
		1500–2000	8%	0%	0.032	0.01	0.013		
		2000–2660	12%	0%	0	0	0.015		
Road Buffer	Meter	<100	53%	60%	1.12	0.15	0.03	0.09	0.004
		100–200	6%	21%	3.54	0.49	0.03		
		200–300	7%	16%	2.28	0.31	0.02		
		300–400	9%	3%	0.33	0.05	0.01		
		400–500	11%	0%	0	0	0		
		>500	14%	0%	0.02	0	0		

Table 2. *Cont.*

Factor	Unit	Class	Class	Landslide	Frequency Ratio (FR)	MFR	FAHP		Consistency Ratio
			%	%			Weights	Factor Weights	
Drainage Buffer	Meter	<100	31%	17%	0.539	0.1	0.031	0.077	0.003
		100–200	14%	24%	1.704	0.31	0.026		
		200–300	16%	20%	1.22	0.22	0.016		
		300–400	18%	17%	0.96	0.17	0.004		
		>400	20%	22%	1.079	0.2	0		
Seismicity	m/s^2	3.5–3.58	17%	16%	0.96	0.18	0	0.03	0.002
		3.59–3.64	19%	53%	2.76	0.52	0		
		3.65–3.71	19%	11%	0.59	0.11	0.01		
		3.72–3.77	20%	20%	0.98	0.19	0.01		
		3.78–3.84	25%	0%	0	0	0.01		
SPI	Ratio	10–20	86%	93%	1.08	0.67	0.007	0.01	0.002
		0–10	14%	7%	0.53	0.33	0.003		
Distance to faults(m)	Meter	300–400	32%	21%	0.66	0.14	0.03	0.069	0.003
		<100	7%	5%	0.72	0.16	0.024		
		100–200	15%	2%	0.13	0.03	0.013		
		200–300	23%	8%	0.37	0.08	0.002		
		>400	23%	63%	2.73	0.59	0		
Rainfall	mm	1297–1325	24%	0%	0	0	0.002	0.104	0.003
		1326–1350	17%	6%	0.37	0.07	0.011		
		1351–1374	20%	19%	0.94	0.19	0.022		
		1375- 1397	17%	14%	0.81	0.17	0.032		
		1398–1419	22%	61%	2.8	0.57	0.037		
TWI	Ratio	0–4	71%	83%	1.16	0.51	0.019	0.029	0.004
		4–8	25%	16%	0.65	0.29	0.01		
		8–12	2%	1%	0.29	0.13	0		
		12–16	2%	0%	0.16	0.07	0		

Table 2. *Cont.*

Factor	Unit	Class	Class	Landslide	Frequency Ratio (FR)	MFR	FAHP		Consistency Ratio
			%	%			Weights	Factor Weights	
NDVI	Ratio	0.50–0.76	11%	0%	0.02	0	0	0.099	0.005
		0.40–0.50	21%	0%	0.02	0	0.011		
		0.3–0.40	36%	9%	0.26	0.02	0.021		
		0.2–0.3	28%	57%	2.01	0.16	0.03		
		<0.20	3%	33%	10.52	0.82	0.037		
Soil	Class	Moderately shallow loamy skeletal soils (excessively drained found on moderately steep slopes)	14%	0%	0.02	0.01	0.001	0.047	0.002
		Moderately deep loamy skeletal soils (excessively drained found on moderately steep slopes)	18%	0%	0	0	0.009		
		Moderately deep coarse loamy soils (well drained found on moderate slopes)	3%	3%	0.89	0.37	0.016		
		Moderately shallow coarse loamy soils (excessively drained found on steep slopes)	65%	97%	1.5	0.62	0.021		
Lithology	Class	Slates (carbonaceous), Quartzite, Stomatolite, Dolomite, and Limestone, micaceous sand with pebbles	9%	3%	0.29	0.15	0.028	0.104	0.004
		Carbonaceous shale, Slate, Greywacke, Clay, Sand, Gravel and Boulders	29%	6%	0.2	0.1	0.007		
		Greywacke, Quartzite, Dolomite, Shale, Dolerite, Limestone, greywacke Conglomerate	62%	92%	1.48	0.75	0.069		

Table 2. *Cont.*

Factor	Unit	Class	Class	Landslide	Frequency Ratio (FR)	MFR	FAHP		Consistency Ratio
			%	%			Weights	Factor Weights	
LULC	Class	River	0%	0%	0	0	0	0.083	0.007
		Sandy area	0%	0%	0	0	0.001		
		Settlement	1%	0%	0	0	0		
		Dense Veg	34%	0%	0.01	0	0.007		
		Plantation	0%	0%	0	0	0.008		
		Agriculture	9%	0%	0	0	0.003		
		Sparse Veg	17%	13%	0.76	0.02	0.013		
		Rocky and Barren land	0%	5%	22.1	0.63	0.019		
		Mining	0%	0%	9.95	0.29	0.02		
		Open and Scrub land	39%	82%	2.08	0.06	0.012		

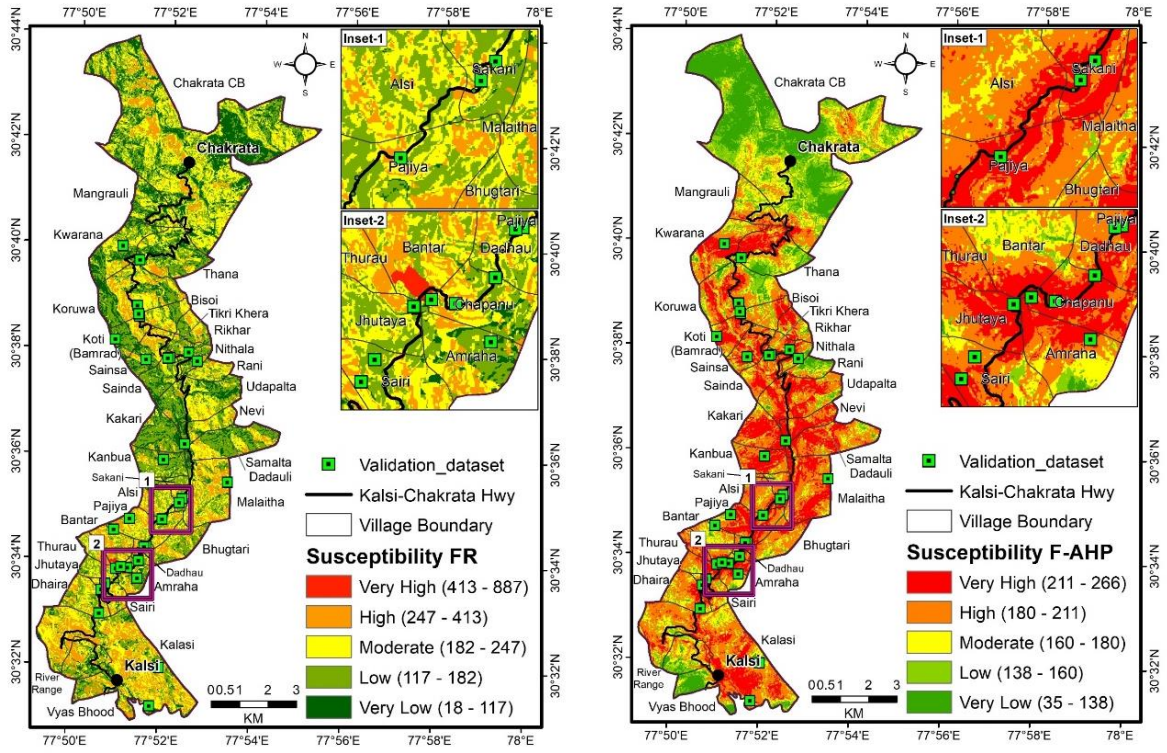

(**a**) (**b**)

Figure 6. LSI Mapping using (**a**) MFR model; (**b**) FAHP model.

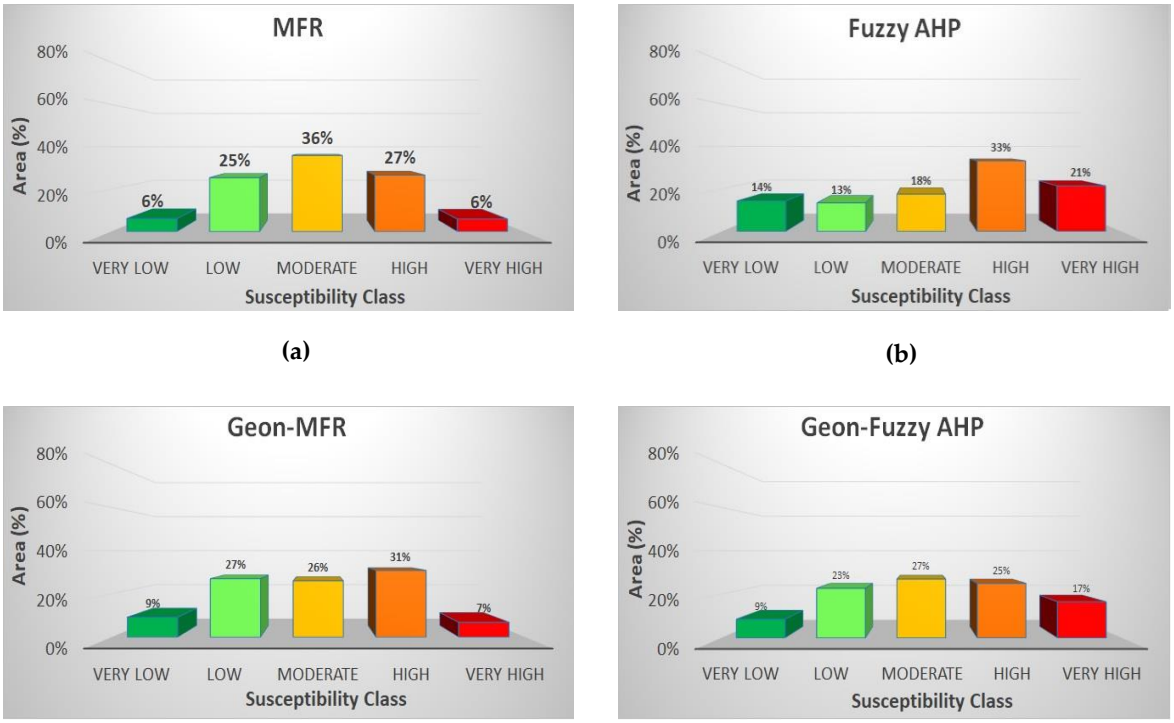

(**a**) (**b**)

(**c**) (**d**)

Figure 7. Percentage area under landslide susceptible zones obtained from the (**a**) MFR; (**b**) FAHP; (**c**) Geon MFR; (**d**) Geon FAHP models.

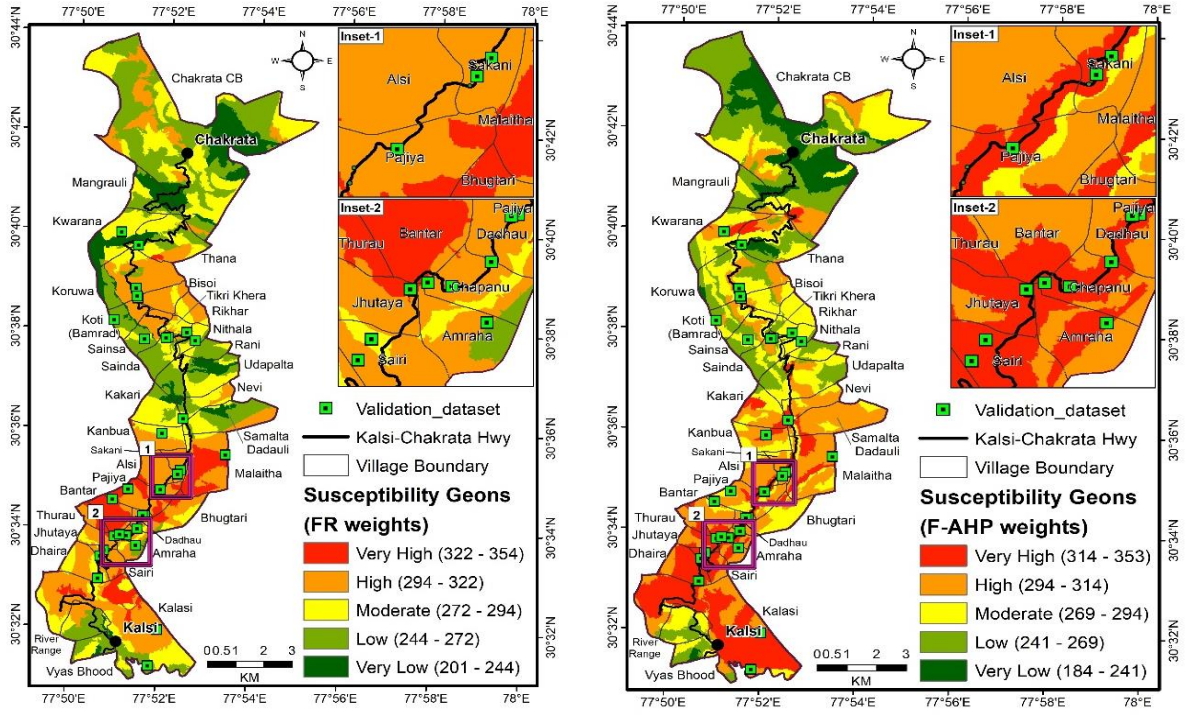

(a) **(b)**

Figure 8. LSI Mapping using (**a**) MFR geons; (**b**) FAHP geons for the Kalsi-Chakrata road corridor.

The village-level landslide susceptibility analysis for the geon MFR model showed that Bantar village is the most susceptible to potential landslides, with 88.34% of its area within the very high LSI class. The next highly susceptible village on the list is Thurau village, with 50.58% of its area within a very high LSI class. On the other hand, the village level landslide hazard analysis of the geon FAHP model showed that Dhaira village and Sairi village, located between Kalsi and Sahiya, are very highly susceptible, with 77.86% and 73.81% of respective village areas falling in that zone.

The geon MFR model output elucidates that among the other villages, Malaitha (47%), Pajiya (47%), and Bhugtari (21%) villages have a greater susceptibility to landslide hazards. Considering collective areas contained by both high and very high LSI zones, Bantar, Pajiya, Thurau, and Alsi have entire village geographical area (100%) under this hazard category, followed by Sakani (99%), Malaitha (91%), and Dadhau (90%). On the other hand, the geon FAHP model output reveals six villages, namely Dhaira, Sairi, Chapanu, Jhutaya, Thurau, and Amroha, where the entire village comes under high and very high LSI zones. Among the other villages having higher landslide susceptible areas are Dadhau, River Range and Bantar.

4.3. Model Validation and Evaluation

4.3.1. Receiver Operating Characteristics (ROC)

As discussed in the Methodology section of this paper, we validated the four LSM output derived from the MFR, FAHP, geon MFR and geon FAHP models through the ROC curve determining the AUC (area under the curve) for each model. The AUC value from the pixel-based MFR model and the FAHP model was 84.1% and 91.0%, respectively, while geon-based MFR and FAHP models show an AUC value of 88.7% and 93.4%, respectively, at 95% confidence level. The validation results indicate higher accuracy of the geon-based models over the MFR and FAHP models in classifying the areas of existing landslides (Figure 9).

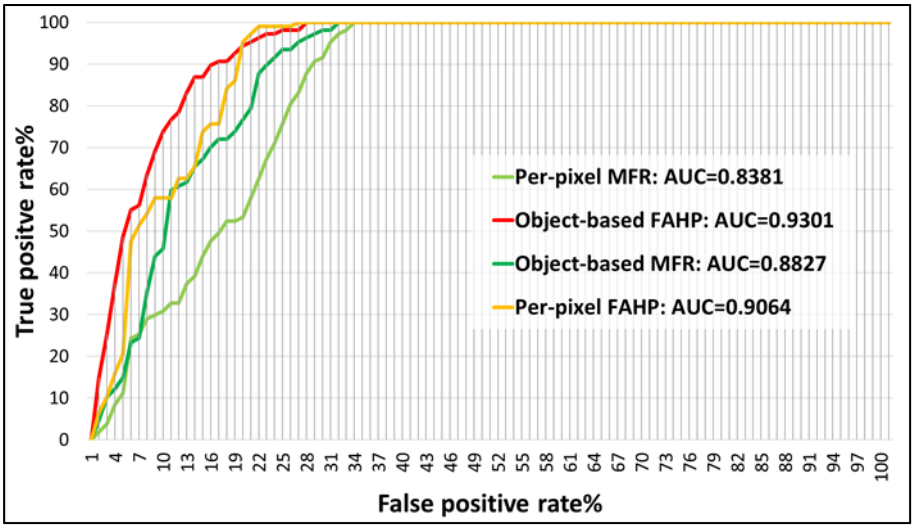

Figure 9. ROC curve showing the precision for the MFR, FAHP, geon MFR and geon FAHP models.

4.3.2. R-Index (Relative Landslide Density)

The model's prediction capability was also verified through the R-index method. Figure 10 below shows the analysis of the R-index plotted as a bar chart to graphically show the consistency of the model's vulnerability assessment. The analysis indicates good consistency of the model results for the defined LSI classes in the present study.

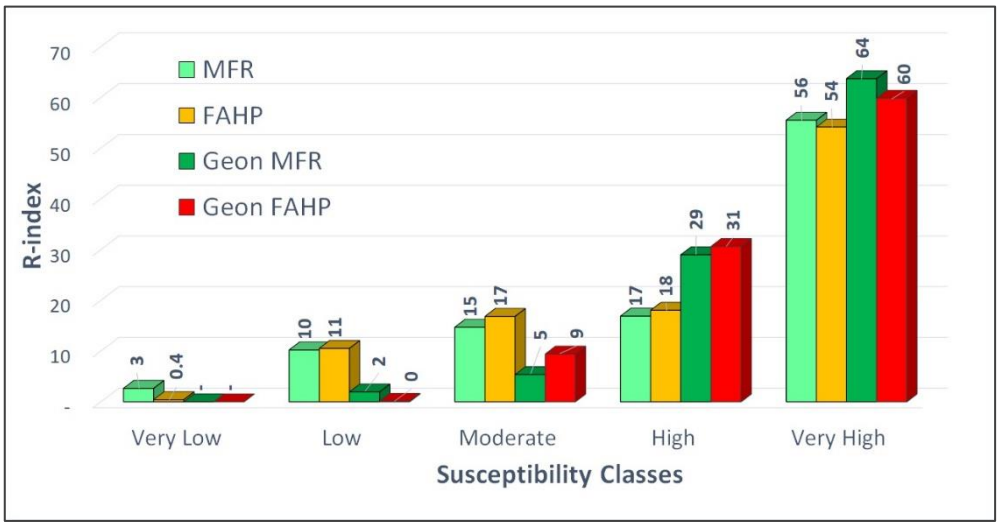

Figure 10. R-Index for LSI Classes.

5. Discussion

This section presents the potential of using the geons concept for LSI mapping in the Lesser Himalayas, applying the per-pixel and object-based aggregation approach. The primary compulsion was to delineate the landslide susceptible areas that are unrestricted by any definite administrative boundaries. As a result, the output susceptibility maps would generate reduced biases developed from artificial (false) limits in an area. Specifically, it indicates the capability of geons to transform continuous spatial data into discrete entities to monitor changes in a specific area. Furthermore, to better understand the mechanism behind the incidence of landslides at a local/regional scale, it is imperative to be familiar with the influence of the landslide conditioning factors at each site.

To better understand the objective of the present study and its adaptability, it would be imperative to briefly overview the landslide studies especially the rainfall-induced

landslides investigations in the Himalayas. A study by [108] indicated that about 15% of the global rainfall-induced significant landslides occurred in Indian Himalayas between 2004–2017. Over the years, a large number of landslide research works have been carried out by scientists and researchers applying techniques ranging from conventional to advanced machine learning methods [109]. Some of these studies focused on the investigation of the main landslide events especially in the Uttarakhand and Himachal Pradesh regions [110–114]. Further, the studies on land-slide were extended to landslide identification, landslide forecasting, lake damming landslides, and, landslides under the impact of climate change by some of the authors [109]. The majority of the studies on the Himalayas in recent years carried out landslide susceptibility mapping (also commonly called landslide hazard zonation mapping) applying qualitative, deterministic, and quantitative techniques. Among these studies, some of the notable ones include knowledge-based qualitative methods [113,115], the deterministic analysis of physical and mechanical properties of the landslide conditioning factors [116,117]. There are also popular semi-quantitative methods based on weights such as AHP (one of the most used methods for Himalayan terrain), weighted linear approaches applied for LSM studies in the Himalayas [118]. As mentioned in the Introduction section of this paper, the quantitative techniques ranging from bi-variate (e.g., frequency ratio, weight of evidence, statistical information value, etc.), multivariate statistical models (e.g., logistic regression) to recent machine learning (ML), support vector machine (SVM) and, artificial neural network (ANN) were adopted by several scholars in their research on the Himalayan landslides. In the past two decades, there has been a few remarkable papers on LSM applying the quantitative techniques published in various journals [5,27,65,119–127].

The geons model in a contemporary quantitative LSM model that allows the users to understand the impact of the conditioning factors on the output LSI values. Hence, geons enable better landslide susceptibility management by distinguishing spatial implementation measures for planners and decision-makers. To make a fair judgment about the efficacy of the LSM models selected for a particular area, comparative studies must evaluate the model performance under the same condition [65,128]. The ROC validation results for LSM output from the MFR, FAHP, geon MFR, and geon FAHP models stipulate that the Geons approach based on the ensemble concept produced better accuracy than the pixel-based LSM techniques. The FAHP approach indicates better predictability than the MFR approach, even when using the ensemble geons method [11]. The inclusion of the fuzzy technique in AHP reduced the biases in the AHP model and enhanced the overall predictability of the model, at least in the present study. Indeed, among the per-pixel models adopted, the FAHP model shows better prediction capability over the MFR model. While the MFR approach is directly based on the correlation between the dependent and independent variables, the FAHP approach is more multifaceted. It needs in-depth subject understanding and skillful judgments to decide the factor weights. In fact, the FAHP model allows the evaluation of the incessant independent variables [65,129].

Studies focus on various approaches and models for LSM in diverse regions, and the outcome of the models vary considerably, resulting in diverse outputs and performances. This study selected the MFR and FAHP models such as the two advanced versions of the traditional per-pixel-based weightage methods to better compare the state-of-the-art ensemble aggregation models as geons (object-based). While the data-oriented MFR method is easier to apply and a simpler approach, the MCDM-based FAHP involves more domain expertise and expert judgement to assign weightages for each landslide conditioning factor. The MFR approach evaluates the relationship between the landslide conditioning factors in a discrete form (comparing the connection between one dependent variable with several independent variables). On the other hand, in addition to the distinct forms, the FAHP approach allows evaluation of continuous independent variables. The same may have attributed to the quite diverse spatial distribution of the landslide susceptibilities in the study area (Figures 6 and 7).

As presented in Table 2, most of the weightages assigned for the sub-criteria in both MFR and FAHP models are diverse in absolute expressions, but they depict likenesses in some classes. For example, the result obtained from the FAHP model describes slope as the utmost influential factor that influences the occurrence of landslides in the study area, having a FAHP weight of 0.110 (Table 2). Based on the obtained weights in descending order, the priorities next to slope are (ii) rainfall, (iii) lithology, (iv) NDVI, (v) aspect, (vi) road proximity, (vii) LULC, (viii) drainage proximity, (ix) fault proximity, (x) altitude, (xi) soil, (xii) seismicity, (xiii) TWI, and (ix) SPI. Indeed, the FAHP indicates that slope angle greater than 50° is amongst the most significant conditioning factors used in the model building. Similarly, some of the significant conditioning factors sub-factors as per their weightages are—NDVI value < 0.2, average annual rainfall >1450 mm, road/drainage/fault proximity within 100 m distance and, lithology sub-class (L1) containing the higher volume of greywacke materials.

The methods adopted in this study may be adopted in different geographical settings with a suitable set of landslide conditioning factors. Such a study will help to compare and assess the model's applicability spatially. Since the performance of a model often varies with the resolution and detailing of the conditioning factors for a region, it may be needed to select a higher resolution and more significant conditioning factors for superior model predictability [16,65,130]. The current geons-based landslide susceptibility approach adopted here can be extended to use in other areas of the globe to test the influence of the conditioning factors under varying conditions that may affect the technique used and its accuracy. The findings of the present work can be utilized by various government and non-government organizations responsible for the development, management, and mitigation of landslide vulnerability in hilly terrains. In the future, the geons method may be integrated with artificial intelligence, and machine learning methods to inspect if the performance of the combined models yield better performance over the other geons based approach adopted in other similar studies.

6. Conclusions

The present study is the first instance of the object-based ensemble geons approach for LSM in the Himalayas mountain range. To date, no in-depth landslide susceptibility analysis has been carried out using ensemble techniques for the mountainous Lesser Himalayan Kalsi-Chakrata road corridor. Therefore, referring to the output of the geon-based models, the decision-makers and regional planners may significantly benefit in selecting the appropriate risk mitigation procedures to counter the potential damages and losses from landslides. The study reveals that the advanced statistical models integrated with RS and GIS methods may be substantial in the spatial prediction of potential landslide occurrence in the said road corridor. The results assessed in the study indicated that all the four models of MFR, FAHP, geon MFR, and geon FAHP performed reasonably well in restricting the landslide susceptible zones. The AUC value in the ROC analysis predicts 93.4% accuracy of the geon FAHP model, which is superior to the three other selected models in this study. The overlay analysis indicates about 41% of the total area within very high and high landslide hazard zones. The validation outcomes indicate that the object-based models can yield higher accuracy compared to the per-pixel based MFR and FAHP approaches, and geon represents meaningful units from planning and mitigation perspective.

Furthermore, by correlating the landslide inventory with the landslide conditioning or influencing factors, we may conclude that rocky and barren areas (covered with sparse vegetation) on the steeper slopes (usually more than 50°) with greywacke type of rocks are more prone to future landslides. Moreover, the heavy torrential rain in the Lesser Himalayan terrain combined with the increased construction activities and vehicular movements has undoubtedly intensified landslides along the road corridor.

The output LSI map in this study was generated from the selected models based on the point location of landslides marked in the field; however, the result might differ if we

consider the landslide inventory drawn as polygon (area). In the future, the geon approach can be integrated with machine learning methods and deep learning techniques.

The present study presents the use of geon as an object-based ensemble approach for landslide susceptibility mapping in the Lesser Himalayas. Hence, the results of this research may be valuable for the planners and local authorities in selecting suitable mitigation measures to minimize the potential landslide hazard damages and losses. This study may offer a substantial prediction procedure for the decision-makers and disaster management officials, and this research may be extended to other road corridors in the Lesser Himalayas similar to the Kalsi-Chakrata area of Uttarakhand.

Author Contributions: Conceptualization, U.S., P.S., S.R.M., T.N.S., Methodology, U.S. and P.S., S.R.M. data processing: U.S., P.S., writing—original draft preparation, U.S., P.S., S.R.M., T.N.S. visualization, U.S., P.S., S.R.M., T.N.S. All authors have read and agreed to the published version of the manuscript.

Funding: This research received no external funding.

Institutional Review Board Statement: Not applicable.

Informed Consent Statement: Not applicable.

Data Availability Statement: Not applicable.

Acknowledgments: We thank to the anonymous reviewers for their constructive and meaningful comments for further improvement of the quality of the manuscript. The work presented is a part of Ph.D. work of first author U.S. under the supervision of P.S.

Conflicts of Interest: The authors declare no conflict of interest.

References

1. Mathew, J.; Jha, V.K.; Rawat, G.S. Weights of evidence modeling for landslide hazard zonation mapping in part of Bhagirathi valley, Uttarakhand. *Curr. Sci.* **2007**, *92*, 628–637.
2. Hong, H.; Pradhan, B.; Xu, C.; Bui, D.T. Spatial prediction of landslide hazard at the Yihuang area (China) using two-class kernel logistic regression, alternating decision tree and support vector machines. *Catena* **2015**, *133*, 266–281. [CrossRef]
3. Nadim, F.; Kjekstad, O.; Peduzzi, P.; Herold, C.; Jaedicke, C. Global landslide and avalanche hotspots. *Landslides* **2006**, *3*, 159–173. [CrossRef]
4. Geological Survey of India, Geological Map. Available online: https://www.gsi.gov.in/webcenter/portal/OCBIS?_afrLoop=50017052507508016&_adf.ctrl-state=1bmlw2iaje_1#!%40%40%3F_afrLoop%3D50017052507508016%26_adf.ctrl-state%3D1bmlw2iaje_5 (accessed on 11 January 2022).
5. Thai Pham, B.; Tien Bui, D.; Prakash, I. Landslide susceptibility modelling using different advanced decision trees methods. *Civ. Eng. Environ. Syst.* **2019**, *35*, 139–157. [CrossRef]
6. Kaur, H.; Gupta, S.; Parkash, S. Comparative Evaluation of Various Approaches for Landslide Hazard Zoning: A Critical Review in Indian Perspectives. *Spat. Inf. Res.* **2017**, *25*, 389–398. [CrossRef]
7. Ambrosi, C.; Strozzi, T.; Scapozza, C.; Wegmuller, U. Landslide hazard assessment in the Himalayas (Nepal and Bhutan) based on Earth-Observation data. *J. Eng. Geol.* **2018**, *237*, 217–228. [CrossRef]
8. Li, Y.; Zhou, R.; Zhao, G.; Li, H.; Su, D.; Ding, H.; Yan, Z.; Yan, L.; Yun, K.; Ma, C. Tectonic uplift and landslides triggered by the Wenchuan earthquake and constraints on orogenic growth: A case study from Hongchun Gully, Longmen Mountains, Sichuan, China. *Quat. Int.* **2014**, *349*, 142–152. [CrossRef]
9. Kwan, J.S.H.; Chan, S.L.; Cheuk, J.C.Y.; Koo, R.C.H. A case study on an open hillside landslide impacting on a flexible rock fall barrier at Jordan Valley, Hong Kong. *Landslides* **2014**, *11*, 1037–1050. [CrossRef]
10. Haque, U.; Da Silva, A.P.F.; Devoli, G.; Pilz, J.; Zhao, B.; Khaloua, A.; Wilopo, W.; Anderson, P.; Ping, L.; Lee, J.; et al. The human cost of global warming: Deadly landslides and their triggers (1995–2014). *Sci. Total Environ.* **2019**, *682*, 673–684. [CrossRef]
11. Sur, U.; Singh, P.; Meena, S.R. Landslide susceptibility assessment in a lesser Himalayan road corridor (India) applying fuzzy AHP technique and earth-observation data. *Geomat. Nat. Hazards Risk* **2020**, *11*, 2176–2209. [CrossRef]
12. Rai, P.K.; Mohan, K.; Kumra, V.K. Landslide hazard and its mapping using Remote Sensing & GIS techniques. *J. Sci. Res.* **2014**, *58*, 1–13.
13. Singh, P.; Sharma, A.; Sur, U.; Rai, P.K. Comparative landslide susceptibility assessment using statistical information value and index of entropy model in Bhanupali-Beri region, Himachal Pradesh, India. *Environ. Dev. Sustain.* **2020**, *23*, 5233–5250. [CrossRef]
14. NASA. Climate change could trigger more landslides in High Mountain Asia. *Science News*, 11 February 2020. Available online: https://www.sciencedaily.com/releases/2020/02/200211121512.htm (accessed on 14 February 2022).

15. Varnes, D.J. *Landslide Hazard Zonation: A Review of Principles and Practice*; Natural Hazards; UNESCO: Paris, France, 1984; Available online: https://www.scirp.org/(S(351jmbntvnsjt1aadkposzje))/reference/ReferencesPapers.aspx?ReferenceID=1768332 (accessed on 11 January 2022).
16. Sur, U.; Singh, P. Landslide Susceptibility Indexing using geospatial and geostatistical techniques along Chakrata-Kalsi road corridor, India. *J. Indian Natl. Cartogr. Assoc. INCA* **2019**, *38*, 2018.
17. Pellicani, R.; van Westen, C.J.; Spilotro, G. Assessing landslide exposure in areas with limited landslide information. *Landslides* **2014**, *11*, 463–480. [CrossRef]
18. Singh, P.; Sharma, A. Probabilistic Landslide susceptibility mapping using binary logistic regression model and Geospatial Techniques: A case study of Uttarakhand. In Proceedings of the 16th ESRI User Conference, New Delhi, India, 2–4 December 2015.
19. Glade, T. Landslide Hazard Assessment and Historical Landslide Data—An Inseparable Couple? The Use of Historical Data in Natural Hazard Assessments. *Adv. Nat. Technol. Hazards Res.* **2001**, *17*, 153–168. [CrossRef]
20. Wang, Y.; Huiming, T.; Wen, T.; Ma, J. Direct Interval Prediction of Landslide Displacements Using Least Squares Support Vector Machines. *Complexity* **2020**, *2020*, 7082594. [CrossRef]
21. Ghorbanzadeh, O.; Blaschke, T.; Aryal, J.; Gholaminia, K. A new GIS-based technique using an adaptive neuro-fuzzy inference system for land subsidence susceptibility mapping. *J. Spat. Sci.* **2018**, 401–418. [CrossRef]
22. Van Westen, C.J.; Rengers, N.; Soeters, R. Use of geomorphological information in indirect landslide susceptibility assessment. *Nat. Hazards* **2003**, *30*, 399–419. [CrossRef]
23. Hasekioğulları, G.D.; Ercanoglu, M. A new approach to use AHP in landslide susceptibility mapping: A case study at Yenice (Karabuk, NW Turkey). *Nat. Hazards* **2012**, *63*, 1157–1179. [CrossRef]
24. Yan, T.; Shen, S.; Zhou, A.; Chen, J. A Brief Report of Pingdi Landslide (23 July 2019) in Guizhou Province, China. *Geosciences* **2019**, *9*, 368. [CrossRef]
25. Tavakkoli Piralilou, S.; Shahabi, H.; Jarihani, B.; Ghorbanzadeh, O.; Blaschke, T.; Gholamnia, K.; Meena, S.R.; Aryal, J. Landslide Detection Using Multi-Scale Image Segmentation and Different Machine Learning Models in the Higher Himalayas. *Remote Sens.* **2019**, *11*, 2575. [CrossRef]
26. Dao, D.V.; Jaafari, A.; Bayat, M.; Mafi-Gholami, D.; Qi, C.; Moayedi, H.; van Phong, T.; Ly, H.-B.; Le, T.-T.; Trinh, P.T.; et al. A spatially explicit deep learning neural network model for the prediction of landslide susceptibility. *Catena* **2020**, *188*, 104451. [CrossRef]
27. Meena, S.R.; Mishra, B.; Tavakkoli, P.S. A hybrid spatial multi-criteria evaluation method for mapping landslide susceptible areas in Kullu Valley, Himalayas. *Geosciences* **2019**, *9*, 156. [CrossRef]
28. Sameen, M.I.; Pradhan, B.; Lee, S. Application of convolutional neural networks featuring Bayesian optimization for landslide susceptibility assessment. *Catena* **2020**, *186*, 104249. [CrossRef]
29. Lee, S.; Pradhan, B. Landslide hazard mapping at Selangor, Malaysia using frequency ratio and logistic regression models. *Landslides* **2007**, *4*, 33–41. [CrossRef]
30. Althuwaynee, O.F.; Pradhan, B.; Lee, S. Application of an evidential belief function model in landslide susceptibility mapping. *Comput. Geosci.* **2012**, *44*, 120–135. [CrossRef]
31. Pourghasemi, H.R.; Pradhan, B.; Gokceoglu, C. Application of fuzzy logic and analytical hierarchy process (AHP) to landslide susceptibility mapping at Haraz watershed, Iran. *Nat. Hazards* **2012**, *63*, 965–996. [CrossRef]
32. Nampak, H.; Pradhan, B.; Manap, M.A. Application of GIS based data driven evidential belief function model to predict groundwater potential zonation. *J. Hydrol.* **2014**, *513*, 283–300. [CrossRef]
33. Meena, S.R.; Ghorbanzadeh, O.; Blaschke, T. A Comparative Study of Statistics-Based Landslide Susceptibility Models: A Case Study of the Region Affected by the Gorkha Earthquake in Nepal. *ISPRS Int. J. Geo-Inf.* **2019**, *8*, 94. [CrossRef]
34. Salvatici, T.; Tofani, V.; Rossi, G.; D'Ambrosio, M.; Tacconi Stefanelli, C.; Masi, E.B.; Rosi, A.; Pazzi, V.; Vannocci, P.; Petrolo, M.; et al. Application of a physically based model to forecast shallow landslides at a regional scale. *Nat. Hazards Earth Syst. Sci.* **2018**, *18*, 1919–1935. [CrossRef]
35. Wang, Q.; Guo, Y.; Li, W.; He, J.; Wu, Z. Predictive modeling of landslide hazards in Wen County, northwestern China based on information value, weights-of-evidence, and certainty factor. *Geomat. Nat. Hazards Risk* **2019**, *10*, 820–835. [CrossRef]
36. Medina, V.; Hürlimann, M.; Guo, Z.; Lloret, A.; Vaunat, J. Fast physically-based model for rainfall-induced landslide susceptibility assessment at regional scale. *Catena* **2021**, *201*, 105213. [CrossRef]
37. Hürlimann, M.; Guo, Z.; Puig-Polo, C.; Medina, V. Impacts of future climate and land cover changes on landslide susceptibility: Regional scale modelling in the Val d'Aran region (Pyrenees, Spain). *Landslides* **2022**, *19*, 99–118. [CrossRef]
38. Kalantar, B.; Pradhan, B.; Naghibi, S.A.; Motevalli, A.; Mansor, S. Assessment of the effects of training data selection on the landslide susceptibility mapping: A comparison between support vector machine (SVM), logistic regression (LR) and artificial neural networks (ANN). *Geomat. Nat. Hazards Risk* **2018**, *9*, 49–69. [CrossRef]
39. Catani, F.; Lagomarsino, D.; Segoni, S.; Tofani, V. Landslide susceptibility estimation by random forests technique: Sensitivity and scaling issues. *Nat. Hazard Earth Syst. Sci.* **2013**, *13*, 2815–2831. [CrossRef]
40. Althuwaynee, O.F.; Pradhan, B.; Ahmad, N. Landslide susceptibility mapping using decision-tree based CHi-squared automatic interaction detection (CHAID) and Logistic regression (LR) integration. *IOP Conf. Ser. Earth Environ. Sci.* **2014**, *20*, 012032. [CrossRef]

41. Althuwaynee, O.F.; Pradhan, B.; Park, H.-J.; Lee, J.H. A novel ensemble decision tree-based CHi-squared Automatic Interaction Detection (CHAID) and multivariate logistic regression models in landslide susceptibility mapping. *Landslides* **2014**, *11*, 1063–1078. [CrossRef]
42. Bi, R.; Schleier, M.; Rohn, J.; Ehret, D.; Xiang, W. Landslide susceptibility analysis based on ArcGIS and Artificial Neural Network for a large catchment in Three Gorges region, China. *Environ. Earth Sci.* **2014**, *72*, 1925–1938. [CrossRef]
43. Park, S.; Choi, C.; Kim, B.; Kim, J. Landslide susceptibility mapping using frequency ratio, analytic hierarchy process, logistic regression, and artificial neural network methods at the Inje area, Korea. *Environ. Earth Sci.* **2013**, *68*, 1443–1464. [CrossRef]
44. Mondal, S.; Maiti, R. Integrating the analytical hierarchy process (AHP) and the frequency ratio (FR) model in landslide susceptibility mapping of Shiv-khola watershed, Darjeeling Himalaya. *Int. J. Disaster Risk Sci.* **2013**, *4*, 200–212. [CrossRef]
45. Razandi, Y.; Pourghasemi, H.R.; Neisani, N.S.; Rahmati, O. Application of analytical hierarchy process, frequency ratio, and certainty factor models for groundwater potential mapping using GIS. *Earth Sci. Inform.* **2015**, *8*, 867–883. [CrossRef]
46. Hay, G.J.; Castilla, G. Geographic Object-Based Image Analysis (GEOBIA): A new name for a new discipline. In *Object-Based Image Analysis*; Springer: Berlin/Heidelberg, Germany, 2008.
47. Li, Y.; Chen, W. Landslide susceptibility evaluation using hybrid integration of evidential belief function and machine learning techniques. *Water* **2020**, *12*, 113. [CrossRef]
48. Zhao, X.; Chen, W. Optimization of computational intelligence models for landslide susceptibility evaluation. *Remote Sens.* **2020**, *12*, 2180. [CrossRef]
49. Banerjee, P.; Ghose, M.K.; Pradhan, R. Analytic Hierarchy Process and Information Value Method based Landslide Susceptibility Mapping and Vehicle Vulnerability Assessment along a highway in Sikkim Himalaya. *Arab. J. Geosci.* **2018**, *11*, 1–18. [CrossRef]
50. Zhao, F.; Meng, X.; Zhang, Y.; Chen, G.; Su, X.; Yue, D. Landslide Susceptibility Mapping of Karakorum Highway Combined with the Application of SBAS-InSAR Technology. *Sensors* **2019**, *19*, 2685. [CrossRef]
51. Hussain, G.; Singh, Y.; Singh, K.; Bhat, G.M. Landslide susceptibility mapping along national highway-1 in Jammu and Kashmir State (India). *Innov. Infrastruct. Solut.* **2019**, *4*, 59. [CrossRef]
52. Anis, Z.; Wissem, G.; Vali, V.; Smida, H.; Essghaier, G.M. GIS-based landslide susceptibility mapping using bivariate statistical methods in North-western Tunisia. *Open Geosci.* **2019**, *11*, 708–726. [CrossRef]
53. Rashid, B.; Iqbal, J. Landslide susceptibility analysis of Karakoram highway using analytical hierarchy process and scoops 3D. *J. Mt. Sci.* **2020**, *17*, 1596–1612. [CrossRef]
54. Pasang, S.; Kubíček, P. Landslide Susceptibility Mapping Using Statistical Methods along the Asian Highway, Bhutan. *Geosciences* **2020**, *10*, 430. [CrossRef]
55. Panchal, S.; Shrivastava, A.K. Landslide hazard assessment using analytic hierarchy process (AHP): A case study of National Highway 5 in India. *Ain Shams Eng. J.* **2021**, *13*, 101626. [CrossRef]
56. Thai Pham, B.; Tien Bui, D.; Prakash, I.; Dholakia, M.B. Landslide Susceptibility Assessment at a Part of Uttarakhand Himalaya, India using GIS–based Statistical Approach of Frequency Ratio Method. *Int. J. Eng. Res. Technol.* **2015**, *4*, 338–344. [CrossRef]
57. Baral, N.; Karna, A.K.; Gautam, S. Landslide Susceptibility Assessment Using Modified Frequency Ratio Model in Kaski District, Nepal. *Int. J. Eng. Manag. Res.* **2021**, *11*, 167–177. [CrossRef]
58. Sur, U.; Singh, P.; Rai, P.K.; Thakur, J.K. Landslide probability mapping by considering fuzzy numerical risk factor (FNRF) and landscape change for road corridor of Uttarakhand, India. *Environ. Dev. Sustain.* **2021**, *23*, 13526–13554. [CrossRef]
59. Das, S.; Sarkar, S.; Kanungo, D.P. GIS-based landslide susceptibility zonation mapping using the analytic hierarchy process (AHP) method in parts of Kalimpong Region of Darjeeling Himalaya. *Environ. Monit. Assess.* **2022**, *194*, 234. [CrossRef] [PubMed]
60. Pradhan, B.; Lee, S. Landslide susceptibility assessment and factor effect analysis: Back propagation artificial neural networks and their comparison with frequency ratio and bivariate logistic regression modeling. *Environ. Model. Softw.* **2010**, *25*, 747–759. [CrossRef]
61. Kumar, R.; Anbalagan, R. Landslide susceptibility zonation in part of Tehri reservoir region using frequency ratio, fuzzy logic and GIS. J. *Earth Syst. Sci.* **2015**, *124*, 431–448. [CrossRef]
62. Khan, H.; Shafique, M.; Khan, M.A.; Bacha, M.A.; Shah, S.U.; Calligaris, C. Landslide susceptibility assessment using frequency ratio, a case study of northern Pakistan. *Egypt. J. Remote Sens. Space Sci.* **2019**, *22*, 11–24. [CrossRef]
63. Mallick, J.; Singh, R.K.; AlAwadh, M.A.; Islam, S.; Khan, R.A.; Qureshi, M.N. GIS-based landslide susceptibility evaluation using fuzzy-AHP multi-criteria decision-making techniques in the Abha Watershed, Saudi Arabia. *Environ. Earth Sci.* **2018**, *77*, 276. [CrossRef]
64. Noorollahi, Y.; Sadeghi, S.; Yousefi, H.; Nohegar, A. Landslide modeling and susceptibility mapping using AHP and fuzzy approaches. *Int. J. Hydrol.* **2018**, *2*, 137–148. [CrossRef]
65. Nachappa, T.G.; Kienberger, S.; Meena, S.R.; Hölbling, D.; Blaschke, T. Comparison and validation of per-pixel and object-based approaches for landslide susceptibility mapping. *Geomat. Nat. Hazards Risk* **2020**, *11*, 572–600. [CrossRef]
66. Chang, D.Y. Application of the extent analysis method on fuzzy AHP. *Eur. J. Oper. Res.* **1996**, *95*, 649–655. [CrossRef]
67. Benz, U.C.; Hofmann, P.; Willhauck, G.; Lingenfelder, I.; Heynen, M. Multi-resolution, object-oriented fuzzy analysis of remote sensing data for GIS-ready information. *ISPRS J. Photogramm. Remote Sens.* **2004**, *58*, 239–258. [CrossRef]
68. Blaschke, T.; Hay, G.J.; Kelly, M.; Lang, S.; Hofmann, P.; Addink, E.; Feitosa, R.Q.; van der Meer, F.; van der Werff, H.; van Coillie, F.; et al. Geographic object-based image analysis–towards a new paradigm. *ISPRS J. Photogramm. Remote Sens.* **2014**, *87*, 180–191. [CrossRef] [PubMed]

69. Lang, S.; Kienberger, S.; Tiede, D.; Hagenlocher, M.; Pernkopf, L. Geons—domain-specific regionalization of space. *Cartogr. Geogr. Inf. Sci.* **2014**, *41*, 214–226. [CrossRef]
70. Khosravi, K.; Panahi, M.; Bui, D.T. Spatial prediction of groundwater spring potential mapping based on an adaptive neuro-fuzzy inference system and metaheuristic optimization. *Hydrol. Earth Syst. Sci.* **2018**, *22*, 4771–4792. [CrossRef]
71. Guzzetti, F.; Mondini, A.C.; Cardinali, M.; Fiorucci, F.; Santangelo, M.; Chang, K.T. Landslide inventory maps: New tools for an old problem. *Earth-Sci. Rev.* **2012**, *112*, 42–66. [CrossRef]
72. Deng, X.; Li, L.; Tan, Y. Validation of spatial prediction models for landslide susceptibility mapping by considering structural similarity. *ISPRS Int. J. Geogr. Inf. Syst.* **2017**, *6*, 103. [CrossRef]
73. Steger, S.; Mair, V.; Kofler, C.; Pittore, M.; Zebisch, M.; Schneiderbauer, S. Correlation does not imply geomorphic causation in data-driven landslide susceptibility modelling—Benefits of exploring landslide data collection effects. *Sci. Total Environ.* **2021**, *776*, 145935. [CrossRef]
74. Marinos, V.; Stoumpos, G.; Papazachos, C. Landslide hazard and risk assessment for a natural gas pipeline project: The case of the Trans Adriatic Pipeline, Albania Section. *Geosciences* **2019**, *9*, 61. [CrossRef]
75. National Remote Sensing Centre (NRSC) Database. Available online: https://www.nrsc.gov.in/EOP_irsdata_DOI/page_1 (accessed on 20 February 2017).
76. Indian Meteorological Department (IMD) Database. Available online: https://mausam.imd.gov.in/ (accessed on 15 June 2016).
77. National Bureau of Soil Survey (NBSS) Database. Available online: https://nbsslup.icar.gov.in/soil-resource-studiessrs/ (accessed on 20 February 2017).
78. Bureau of Indian Standards (BIS) Database. Available online: https://pib.gov.in/PressReleasePage.aspx?PRID=1740656 (accessed on 20 February 2017).
79. U.S. Geological Survey (USGS) Database. Available online: https://earthquake.usgs.gov/data/vs30/ (accessed on 15 June 2016).
80. Sur, U.; Singh, P. Assessment of Landscape Change of Lesser Himalayan Road Corridor of Uttarakhand, India. *J. Landsc. Ecol.* **2020**, *13*, 1–22. [CrossRef]
81. Zhang, J.; He, P.; Xiao, J.; Xu, F. Risk assessment model of expansive soil slope based on Fuzzy-AHP method and its engineering application. *Geomat. Nat. Hazards Risk* **2018**, *9*, 389–402. [CrossRef]
82. Tien Bui, D.; Pradhan, B.; Revhaug, I.; Nguyen, D.B.; Pham, H.V.; Bui, Q.N. A novel hybrid evidential belief function-based fuzzy logic model in spatial prediction of rainfall-induced shallow landslides in the Lang Son city area (Vietnam). *Geomat. Nat. Hazards Risk* **2015**, *6*, 243–271. [CrossRef]
83. Xu, C.; Xu, X.; Shen, L.; Yao, Q.; Tan, X.; Kang, W.; Ma, S.; Wu, X.; Cai, J.; Gao, M.; et al. Optimized volume models of earthquake-triggered landslides. *Sci. Rep.* **2016**, *6*, 29797. [CrossRef] [PubMed]
84. Liu, S.; Yin, K.; Zhou, C.; Gui, L.; Liang, X.; Lin, W.; Zhao, B. Susceptibility Assessment for Landslide Initiated along Power Transmission Lines. *Remote Sens.* **2021**, *13*, 5068. [CrossRef]
85. Meena, S.R.; Ghorbanzadeh, O.; van Westen, C.J.; Nachappa, T.G.; Blaschke, T.; Singh, R.P.; Sarkar, R. Rapid mapping of landslides in the Western Ghats (India) triggered by 2018 extreme monsoon rainfall using a deep learning approach. *Landslides* **2021**, *18*, 1937–1950. [CrossRef]
86. Chen, W.; Chai, H.; Sun, X.; Wang, Q.; Ding, X.; Hong, H. A GIS-based comparative study of frequency ratio, statistical index and weights-of-evidence models in landslide susceptibility mapping. *Arab. J. Geosci.* **2016**, *9*, 1–16. [CrossRef]
87. Abedini, M.; Tulabi, S. Assessing LNRF, FR, and AHP models in landslide susceptibility mapping index: A comparative study of Nojian watershed in Lorestan province, Iran. *Environ. Earth Sci.* **2018**, *77*, 405. [CrossRef]
88. Li, L.; Lan, H.; Guo, C.; Zhang, Y.; Li, Q.; Wu, Y. A modified frequency ratio method for landslide susceptibility assessment. *Landslides* **2016**, *14*, 727–741. [CrossRef]
89. Althuwaynee, O.F.; Pradhan, B.; Lee, S. A novel integrated model for assessing landslide susceptibility mapping using CHAID and AHP pair-wise comparison. *Remote Sens.* **2016**, *37*, 1190–1209. [CrossRef]
90. Sifa, S.F.; Mahmud, T.; Tarin, M.A.; Haque, D.M.E. Event-based landslide susceptibility mapping using weights of evidence (WoE) and modified frequency ratio (MFR) model: A case study of Rangamati district in Bangladesh. *Geol. Ecol. Landsc.* **2019**, 222–235. [CrossRef]
91. Saaty, T.L. How to make a decision: The analytic hierarchy process. *Eur. J. Oper. Res.* **1990**, *48*, 9–26. [CrossRef]
92. Ayhan, M.B. A Fuzzy AHP approach for supplier selection problem: A case study in a Gearmotor Company. *Intl. J. Manag. Value Supply Chains IJMVSC* **2013**, 4. [CrossRef]
93. Laarhoven, P.V.; Pedrycz, W. A fuzzy extension of Saaty's priority theory. *Fuzzy Sets Syst.* **1983**, *11*, 199–227. [CrossRef]
94. Chen, V.Y.C.; Lien, H.P.; Liu, C.H.; Liou, J.J.H.; Tzeng, G.H.; Yang, L.S. Fuzzy MCDM approach for selecting the best environment-watershed plan. *Appl. Soft Comput.* **2011**, *11*, 265–275. [CrossRef]
95. Feizizadeh, B.; Roodposhti, M.S.; Jankowski, P.; Blaschke, T. A GIS-based extended fuzzy multi-criteria evaluation for landslide susceptibility mapping. *Comput. Geosci.* **2014**, *73*, 208–221. [CrossRef]
96. Shu, H.; Guo, Z.; Qi, S.; Song, D.; Pourghasemi, H.R.; Ma, J. Integrating Landslide Typology with Weighted Frequency Ratio Model for Landslide Susceptibility Mapping: A Case Study from Lanzhou City of Northwestern China. *Remote Sens.* **2021**, *13*, 3623. [CrossRef]

97. Abdi, A.; Bouamrane, A.; Karech, T.; Dahri, N.; Kaouachi, A. Landslide Susceptibility Mapping Using GIS-based Fuzzy Logic and the Analytical Hierarchical Processes Approach: A Case Study in Constantine (North-East Algeria). *Geotech. Geol. Eng.* **2021**, *39*, 5675–5691. [CrossRef]
98. Li, L.; Shi, Z.; Yin, W.; Zhu, D.; Ng, S.L.; Cai, C.; Lei, A. A fuzzy analytic hierarchy process (FAHP) approach to eco-environmental vulnerability assessment for the Danjiangkou Reservoir area, China. *Ecol. Model.* **2009**, *220*, 3439–3447. [CrossRef]
99. Hagenlocher, M.; Kienberger, S.; Lang, S.; Blaschke, T. Implications of spatial scales and reporting units for the spatial modelling of vulnerability to vector-borne diseases. *GI_Forum* **2014**, *197*.
100. Tiede, D.; Lang, S.; Albrecht, F.; Hölbling, D. Object-Based Class Modeling for Cadastre Constrained Delineation of Geo-Objects. *Photogramm. Eng. Remote Sens.* **2010**, *2*, 193–202. [CrossRef]
101. Baatz, M.; Schäpe, A. Multiresolution Segmentation: An Optimization Approach for High Quality Multi-scale Image Segmentation. In *Angewandte Geographische Informationsverarbeitung XII*; Herbert Wichmann: Heidelberg, Germany, 2000.
102. Blaschke, T. Object Based Image Analysis for Remote Sensing. *ISPRS J. Photogramm. Remote Sens.* **2010**, *65*, 2–16. [CrossRef]
103. Drăguţ, L.; Csillik, O.; Eisank, C.; Tiede, D. Automated Parameterisation for Multi-Scale Image Segmentation on Multiple Layers. *ISPRS J. Photogramm. Remote Sens.* **2014**, *88*, 119–127. [CrossRef] [PubMed]
104. Kienberger, S.; Lang, S.; Zeil, P. Spatial Vulnerability Units—Expert-Based Spatial Modelling of Socio-Economic Vulnerability in the Salzach Catchment, Austria. *Nat. Hazards Earth Syst. Sci.* **2009**, *9*, 767–778. [CrossRef]
105. Drăguţ, L.; Tiede, D.; Levick, S.R. ESP: A tool to estimate scale parameter for multiresolution image segmentation of remotely sensed data. *Int. J. Geogr. Inf. Sci.* **2010**, *24*, 859–871. [CrossRef]
106. Pourghasemi, H.R.; Rahmati, O. Prediction of the landslide susceptibility: Which algorithm, which precision? *Catena* **2018**, *162*, 177–192. [CrossRef]
107. Qianqian, B.; Yumin, C.; Susa, D.; Qianjiao, W.; Jiaxin, Y.; Jingyi, Z. An improved information value model based on gray clustering for landslide susceptibility mapping. *ISPRS Int. J. Geo-Inf.* **2017**, *6*, 18. [CrossRef]
108. Froude, M.J.; Petley, D. Global fatal landslide occurrence from 2004 to 2016. *Nat. Hazards Earth Syst. Sci.* **2018**, *18*, 2161–2181. [CrossRef]
109. Dikshit, A.; Sarkar, R.; Pradhan, B.; Segoni, S.; Alamri, A.M. Rainfall Induced Landslide Studies in Indian Himalayan Region: A Critical Review. *Appl. Sci.* **2020**, *10*, 2466. [CrossRef]
110. Kanungo, D.P.; Sharma, S. Rainfall thresholds for prediction of shallow landslides around Chamoli-Joshimath region, Garhwal Himalayas, India. *Landslides* **2014**, *11*, 629–638. [CrossRef]
111. Dikshit, A.; Satyam, D.N. Estimation of rainfall thresholds for landslide occurrences in Kalimpong, India. *Innov. Infrastruct. Solut.* **2018**, *3*, 24. [CrossRef]
112. Kumar, V.; Gupta, V.; Jamir, I. Hazard evaluation of progressive Pawari landslide zone, Satluj valley, Himachal Pradesh, India. *Nat. Hazards* **2018**, *93*, 1029–1047. [CrossRef]
113. Anbalagan, R. Landslide hazard evaluation and zonation mapping in mountainous terrain. *Eng. Geol.* **1992**, *32*, 269–277. [CrossRef]
114. Banerjee, A.; Dimri, A.P. Comparative analysis of two rainfall retrieval algorithms during extreme rainfall event: A case study on cloudburst, 2010 over Ladakh (Leh), Jammu and Kashmir. *Nat. Hazards* **2019**, *97*, 1357–1374. [CrossRef]
115. Gupta, P.; Anbalagan, R. Slope stability of Tehri Dam Reservoir Area, India, using landslide hazard zonation (LHZ) mapping. *Q. J. Eng. Geol.* **1997**, *30*, 27–36. [CrossRef]
116. Mathew, J.; Kundu, S.; Kumar, K.V.; Pant, C.C. Hydrologically complemented deterministic slope stability analysis in part of Indian Lesser Himalaya. *Geomat. Nat. Hazards Risk* **2016**, *7*, 1557–1576. [CrossRef]
117. Sarkar, S.; Roy, A.K.; Raha, P. Deterministic approach for susceptibility assessment of shallow debris slide in the Darjeeling Himalayas, India. *Catena* **2016**, *142*, 36–46. [CrossRef]
118. Kanungo, D.; Arora, M.; Gupta, R.; Sarkar, S. Landslide risk assessment using concepts of danger pixels and fuzzy set theory in Darjeeling Himalayas. *Landslides* **2008**, *5*, 407–416. [CrossRef]
119. Ghosh, S.; Carranza, E.J.M.; van Westen, C.J.; Jetten, V.G.; Bhattacharya, D.N. Selecting and weighting spatial predictors for empirical modeling of landslide susceptibility in the Darjeeling Himalayas (India). *Geomorphology* **2011**, *131*, 35–56. [CrossRef]
120. Das, I.; Stein, A.; Kerle, N.; Dadhwal, V.K. Landslide susceptibility mapping along road corridors in the Indian Himalayas using Bayesian logistic regression models. *Geomorphology* **2012**, *179*, 116–125. [CrossRef]
121. Mandal, S.; Mandal, K. Modeling and mapping landslide susceptibility zones using GIS based multivariate binary logistic regression (LR) model in the Rorachu river basin of eastern Sikkim Himalaya, India. *Modeling Earth Syst. Environ.* **2018**, *4*, 69–88. [CrossRef]
122. Ramakrishnan, D.; Singh, T.N.; Verma, A.K.; Gulati, A.; Tiwari, K.C. Soft computing and GIS for landslide susceptibility assessment in Tawaghat area, Kumaon Himalaya, India. *Nat. Hazards* **2013**, *65*, 315–330. [CrossRef]
123. Roy, J.; Saha, S.; Arabameri, A.; Blaschke, T.; Tien Bui, D. A Novel Ensemble Approach for Landslide Susceptibility Mapping (LSM) in Darjeeling and Kalimpong Districts, West Bengal, India. *Remote Sens.* **2019**, *11*, 2866. [CrossRef]
124. Batar, A.K.; Watanabe, T. Landslide Susceptibility Mapping and Assessment Using Geospatial Platforms andWeights of Evidence (WoE) Method in the Indian Himalayan Region: Recent Developments, Gaps, and Future Directions. *ISPRS Int. J. Geo-Inf.* **2021**, *10*, 114. [CrossRef]

125. Ram, P.; Gupta, V. Landslide hazard, vulnerability, and risk assessment (HVRA), Mussoorie township, lesser himalaya, India. *Environ. Dev. Sustain.* **2022**, *24*, 473–501. [CrossRef]
126. Meghanadh, D.; Mauriya, V.K.; Tiwari, A.; Dwivedi, R. A multi-criteria landslide susceptibility mapping using deep multi-layer perceptron network: A case study of Srinagar-Rudraprayag region (India). *Adv. Space Res.* **2022**, *69*, 1883–1893. [CrossRef]
127. Meena, S.R.; Soares, L.P.; Grohmann, C.H.; van Westen, C.; Bhuyan, K.; Singh, R.P.; Floris, M.; Catani, F. Landslide detection in the Himalayas using machine learning algorithms and U-Net. *Landslides* **2022**, *19*, 1209–1229. [CrossRef]
128. Goetz, J.; Brenning, A.; Petschko, H.; Leopold, P. Evaluating machine learning and statistical prediction techniques for landslide susceptibility modeling. *Comput. Geosci.* **2015**, *81*, 1–11. [CrossRef]
129. Schicker, R.; Moon, V. Comparison of bivariate and multivariate statistical approaches in landslide susceptibility mapping at a regional scale. *Geomorphology* **2012**, *161*, 40–57. [CrossRef]
130. Donati, L.; Turrini, M.C. An objective method to rank the importance of the factors pre- disposing to landslides with the GIS methodology: Application to an area of the Apennines (Valnerina; Perugia, Italy). *Eng. Geol.* **2002**, *63*, 277–289. [CrossRef]